Fluid and Thermodynamic Underhood Simulations

Begoña León Moya

Thesis for the Degree of Master of Science

Division of Fluid Mechanics

Department of Energy Sciences

Faculty of Engineering

Lund University

CFD is like a dog walking on its hind legs; it's doing it badly, but it's amazing that it can do it at all

- *Anonymous*

Nothing in life is to be feared, it is only to be understood. Now is the time to understand more, so that we may fear less.

- Marie Curie

Abstract

The thermal model and simulation of vehicles components is necessary within the development phase of the vehicle production process. It is important to understand the thermal processes of high temperature components in the vehicle, such as the exhaust system.

The exhaust system presents a high thermal activity that increases the temperature of the exhaust system itself and the nearby surrounding engine components, due to the large amount of heat transferred by radiation.

The aim of this thesis is to develop a method that predicts the surface temperature of the exhaust system to ensure that no component overheats. This method includes coupling CFD software with heat transfer software.

This model was validated against a tunnel test proving that the steady-state simulations match closely with the tunnel test data, while taking into consideration the possible sources of errors and discrepancies. Furthermore, a sensitivity analysis is performed in order to evaluate the robustness of the method.

In conclusion, this thesis showed the feasibility of coupling a thermal model with a CFD model to successfully simulate the temperature of the exhaust system and surrounding engine components. This modeling process allows modifying the design without involving new experimental tests, contributing to a reduction of both time and cost. Consequently, this method will be used in future projects within the VCC verification efficiency processes.

Acknowledgements

This thesis has been performed at Volvo Car Corporation in Gothenburg in cooperation with the Department of Energy Science at the Lund Institute of Technology.

I would like to thank the fantastic people from the CFD department for welcoming me to their family. During these months I realized how important it is to enjoy yourself and have fun while you are working. Thanks to all of you for your help and the great fika times. You made this time at Volvo an amazing experience.

I especially would like to thank my supervisors Patrik Sondell and Anders Björtin for guiding me during these months. You showed me how important it is to work in a group and trust the people around you. Thanks for giving me a vote of confidence; I would never have finished this thesis without your support.

I wish to thank Steven Patterson of ThermoAnalytics, Inc. for his technical help during this research.

Thanks also to Jordi, Lennert and Mike for helping me whenever I needed it. You have gone from being my colleagues to being my friends.

Nomenclature

Acronyms

CFD= Computational Fluid Dynamic

DOC = Diesel Oxidation Catalyst

DPF= Diesel Particulate Filter

CAF= Convective Augmentation Factor

EGR= Exhaust Gas Recirculation

HCTR= Hill Climbing Trailer

AR = Aspect Ratio

CAE= Computer-Aided Engineering

Nomenclature

A= Cross-section area [m^2]

h =Heat transfer coefficient [W/m^2K]

$h_{c_{is}}$ = Compressor isentropic mass enthalpy [J/kg]

h_c =Compressor mass enthalpy [J/kg]

h_c =Conductance[W/m^2K]

*m*oles = Mol flow rate [mol/s]

$\dot{m}_{gas}$= Mass flow rate [kg/s]

m = Mass [kg]

P = Pressure [Pa]

P_C = Compressor Power [W]

P_w = Wetter perimeter

Q= Heat transfer rate [W]

R= Resistance [m^2K/W]

T_S = Surface temperature [K]

T_a = Ambient air temperature

T_∞ = Fluid temperature [K]

T = Temperature [K]

u =Velocity vector [m/s]

$\dot{V}_{exhaust\_gas}$ = Volumetric flow rate [m^3/s]

V= Volume [m^3]

W= Work [W]

x =Thickness [m]

ρ =Density [kg/m^3]

v =Kinematic viscosity [m^2/s]

μ =Dynamic viscosity [kg/ms]

κ =Thermal conductivity [W/mK]

ε =emissivity

σ = Stefan-Boltzmann constant [W/m^2K^4]

Re = Reynolds number

R_c= Contact resistance [m^2K/W]

Pr = Prandtl number

D_h= Hydraulic diameter

f = Darcy friction factor

η_{c_O} = Compressor/Turbine efficiency

$\delta_{m,turbo}$= Thickness of the turbulent boundary layer [m]

Table of contents

1.Introduction

1.1. Background

The thermal model and simulation of the vehicle components is very important in the design, optimization and management of vehicle power systems. It is necessary to determine the vehicle parts that present the highest temperature and the heat transferred between these parts.

The exhaust system contains much thermal activity due to the high temperature of the exhaust gas flowing through the system and chemical reaction in the catalytic converter. Therefore, a method development of the exhaust system temperatures is necessary to ensure that no component overheats.

One of the aims of developing this method is to increase the efficiency of the verification process. The method is based on CAE tools currently used at Volvo Cars Corporation for underhood thermal management (Fluent for CFD analysis and RadTherm for Heat Transfer Analysis).

The method developed in this thesis allows modifying the design, adding heat shields or changing the material of the components without involving new experimental tests.

1.2. Objective

The objective of this thesis is to develop a method that predicts the surface temperature of the exhaust system. The exhaust system modeled consists of the manifold, turbo, catalytic converter and ends with an exhaust pipe.

It is important to develop a method of the exhaust system due to the large amount of heat radiated from its surfaces to the nearby surrounding engine components.

The method includes coupling a CFD (convection heat transfer) software with a heat transfer software (radiation and conduction heat transfer) that models the 1-D flow inside the exhaust system

2.Theory

2.1 What is CFD?

Computational Fluid Dynamics (CFD) is a branch within fluid mechanics that applies numerical methods and algorithms to analyze problems related to fluid flow. CFD allows performing detailed calculations of any system in which fluids are involved, by solving the Navier-Stokes [1] equations of conservation of mass, energy and momentum to the particular geometry of each system considered. The non-conserved forms of Navier-Stokes equations are shown below.

Mass
$$\frac{\partial \rho}{\partial t} + u_i \frac{\partial \rho}{\partial x_i} + \rho \frac{\partial u_i}{\partial x_i} = 0 \quad (1)$$

Momentum
$$\rho \frac{\partial u_i}{\partial t} + \rho u_j \frac{\partial u_i}{\partial x_j} = \rho f_i - \frac{\partial p}{\partial x_j} + \frac{\partial \tau_{ij}}{\partial x_j} \quad (2)$$

Energy
$$\rho \frac{\partial E}{\partial t} + \rho u_i \frac{\partial E}{\partial x_i} = \rho \frac{\partial q}{\partial t} + \frac{\partial}{\partial x_i}\left(k \frac{\partial T}{\partial x_i} \right) + \frac{\partial u_j \partial \tau_{ij}}{\partial x_i} - \frac{\partial u_i p}{\partial xi} + \rho u_i f_i \quad (3)$$

Where τ_{ij} are the shear stresses and f_i are the body forces. The results are the values of all the variables that characterize the system (such as speed, pressure, temperature, composition, etc. ...) in each of the points. These simulations allow a new perspective on the problem that is not possible using traditional methods.

The numerical simulation has been gradually replacing the experimental methods used for a long time in several areas. Currently CFD is applied to many fields of engineering, including both mechanical and chemical or medical technology.

2.2 Heat Transfer Methodology

It is important to understand the heat transfer modes and the equations used in this model [2].

Conduction

The heat transfer by conduction happens due to a temperature gradient across a medium. Fourier's Law governs the conduction heat transfer and the heat transfer occurs in the direction of decreasing temperature.

Considering the exhaust system wall shown in Figure 1 with $T_{s1}>T_{s2}$, the temperature difference causes conduction heat transfer in the positive x-direction. The heat transfer rate (Q_{cond}) depends on the temperature difference ΔT; the wall thickness (x); the cross-sectional area (A); and the material conductivity (κ). The conductivity is a coefficient introduced in order to measure the material behavior.

Therefore, the one-dimensional conduction heat transfer through the exhaust wall can be calculated as shown in equation (4).

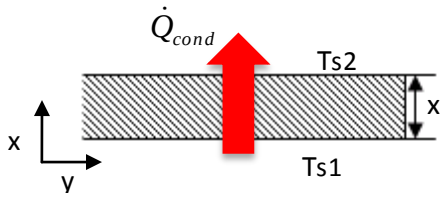

Figure 1. Heat transfer through the exhaust system wall

$$\dot{Q}_{cond} = \frac{\kappa \cdot A}{x} \cdot (T_{S1} - T_{S2}) \quad (4)$$

Convection

Heat transfer by convection occurs due to energy transfer between a surface and a fluid moving over the surface.

According to the nature of the flow, the convection heat transfer is classified in forced and natural convection. Forced convection occurs when the flow is induced by external means, such as a pump or a fan. Natural or free convection is caused by buoyancy forces, caused by density differences.

Figure 2 shows a simple case used to explain convection heat transfer considering a fluid flowing over a heated surface. A region in the fluid, called the *hydrodynamic boundary layer*, is developed due to the interaction between the fluid and the surface. The velocity inside this region varies from zero at the surface to a finite value u_∞. Furthermore, a *thermal boundary layer* is developed due to the temperature difference between the fluid and the surface. The size of this layer may not be the same as that of the hydrodynamic layer.

The convection heat transfer occurs due to the random molecular movement and the bulk motion of the fluid within the boundary layer. Near the surface, where the velocity of the fluid is low, the molecular diffusion dominates. The layer grows as the flow progresses in the x-direction, which leads to a contribution of the bulk fluid motion.

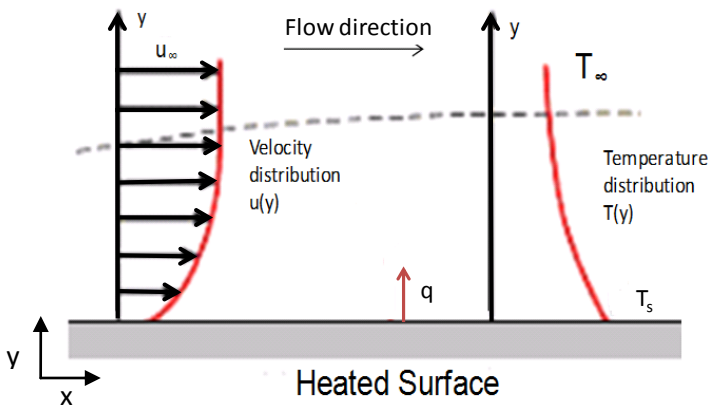

Figure 2. Fluid over a flat plate. Velocity and temperature distribution over the y direction

During the boundary layer development, the flow can be laminar and turbulent in many cases where the laminar section precedes the turbulent section. The laminar flow is greatly ordered and streamlines can be seen along this section. The ordered flow continues until it reaches the transition zone where the flow passes from a laminar to a turbulent flow. The turbulent flow is mainly random and highly irregular, which contributes to a mixing within the boundary layers. The mixing is mainly caused by the streamwise vortices close to the flat plate.

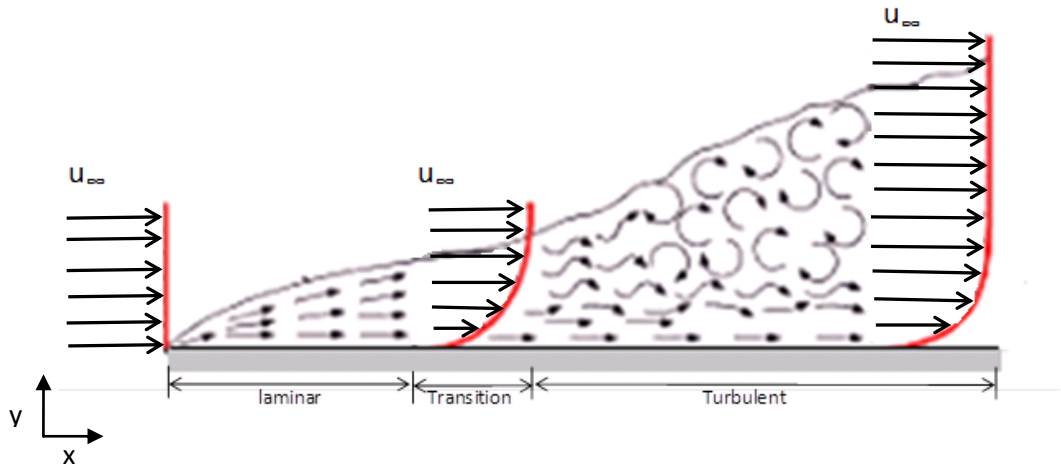

Figure 3. Velocity boundary layer development in a flat plate

The transition from laminar to turbulent flow depends on the triggering mechanisms. The turbulent flow is reached depending on if the triggering mechanism is amplified or diminished in the direction of the fluid flow. A dimensionless number called the Reynolds number is used to characterize the flow regime. Low Reynolds numbers involves a laminar flow where the viscous forces are dominant. On the contrary, high Reynolds numbers contribute to a turbulent flow where the inertial forces dominate.

The fluid flow is divided into internal and external flow. The internal flow is defined as one where the growth of the boundary layer is confined [3] and the external flow is defined as one where the boundary layer can grow without bounds.

The Reynolds number that characterized the external flow is based on the free-stream velocity and characteristic length (x), which is the distance from the leading edge.

$$\mathrm{Re} = \frac{\rho \cdot u_{\infty} \cdot x}{\mu} \quad (5)$$

An external flow becomes turbulent when the Reynolds number is higher than $5x10^5$.

The Reynolds number that characterizes the internal flow is based on the mean velocity (or bulk velocity) and the hydraulic diameter, D_h, which is the characteristic dimension of the duct cross-section.

$$\mathrm{Re} = \frac{\rho \cdot u_m \cdot D_h}{\mu} \quad (6)$$

The hydraulic diameter is calculated as shown in equation (7).

$$D_h = \frac{4 \cdot A_c}{P_w} \quad (7)$$

where P_w is the wetted perimeter of the duct, defined as the perimeter in contact with the fluid.The critical Reynolds number for internal flow is usually assumed to be 2300.

The thermally developing region is where the thermal boundary layers are growing, whereas the region where the thermal boundary layers are bounded is called the thermally fully developed region. A turbulent flow will become fully developed when the boundary layer emerges across the half-width of the duct [4].

$$\delta_{\mathrm{m,turbo}} \approx \frac{D_h}{2} \approx 0.16 \cdot x_{fd,h,turbo} \cdot \left(\frac{\rho \cdot u_{\infty} \cdot x_{fd,h,turbo}}{\mu}\right)^{-1/7} \quad (8)$$

Regardless of the nature of the convection process, the heat transfer rate by convection is calculated as follows.

$$Q_{conv} = h_{conv} \cdot A \cdot (T_f - T_s) \quad (9)$$

where Q_{con} is the convection heat transfer rate, T_f is the fluid temperature and the T_s is the surface temperature. The h_{conv} is the convection heat transfer coefficient and it depends on the conditions in the boundary layer, which are influence by surface geometry, the nature of the fluid diffusivity, and other transport and thermodynamic properties of the fluid. Convection coefficients are frequently correlated using the local Nusselt number that is based on the hydraulic diameter.

$$Nu = \frac{h \cdot D_h}{\kappa} \quad (10)$$

The Nusselt number is correlated by the Reynolds number, the relative roughness and the Prandtl Number. For internal flows, Nu can usually be expressed as shown in equation (11).

$$Nu = a \cdot \mathrm{Re}^{b} \cdot \mathrm{Pr}^{c} \quad (11)$$

where a, b and c are arbitrary constants and Pr is the Prandtl number. The Prandtl number is a dimensionless number that relates the ratio of the momentum diffusivity and the thermal diffusivity as shown in equation (12)

$$\mathrm{Pr} = \frac{C_p \cdot \mu}{\kappa} \quad (12)$$

Nusselt number is usually calculated by correlations based on experiments. The correlations used in this model are described in Appendix A.

Radiation

The thermal radiation is defined as the energy emitted from a body having a temperature other than zero. Unlike conduction and convection, radiation does not require the presence of a material to be propagated. In this case, the energy of the radiation is transported by electromagnetic waves.

The heat emitted by a body is defined as follows,

$$E = \varepsilon \sigma T^{4} \quad (13)$$

where ε is the emissivity and the σ is the Stefan-Boltzmann constant. The emissivity is a property that depends on the surface material and it can vary from 0 to 1 depending on how efficient a body is in comparison with a black body that represents an emissivity of 1.

Equation 14 shows the radiation exchange between two surfaces at two different temperatures assuming they are isothermal surfaces.

$$Q_{radiation} = \varepsilon \cdot \sigma \cdot A \cdot (T_1^4 - T_2^4) \quad (14)$$

where T_1 and T_2 are the two surface temperatures

The heat transfer in the exhaust system can be divided into:

- Forced convection heat transfer between the exhaust system and the surrounding air.
- Radiation to surrounding parts.
- Conduction with all the connecting parts.
- Forced convection heat transfer between the exhaust system and the exhaust gas.

Assuming a simple one-dimensional heat transfer shown in Figure 4.The external heat transfer, the conduction and the internal heat transfer in the exhaust system can be defined as follows,

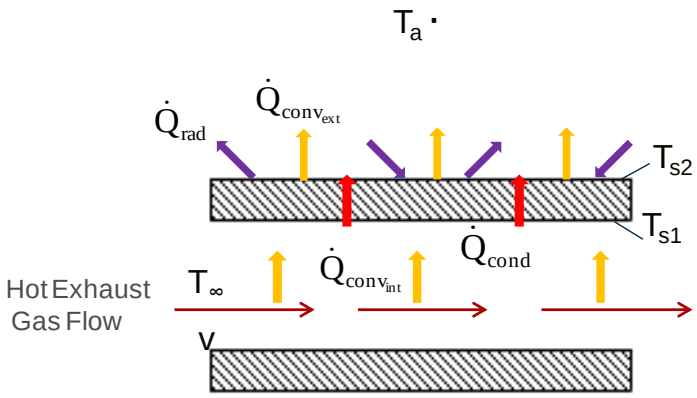

Figure 4. Heat transfer in the exhaust system

$$\dot{Q}_{ext} = Q_{conv} + Q_{rad} = h_s A_S (T_{S2} - T_a) + \varepsilon\sigma A_s (T_{S2}^4 - T_a^4) \quad (15)$$

$$Q_{cond} = \frac{\kappa \cdot A}{t} \cdot (T_{S1} - T_{S2}) \quad (16)$$

$$Q_{\text{int}} = h_{\text{int}} \cdot A \cdot (T_f - T_{s1}) \quad (17)$$

It is important to notice that the fluid in the developed exhaust model corresponds to exhaust gas with a pulsating nature. Several experiments show that the heat transfer rates in exhaust gases are higher than expected due to the pulsating nature of the flow in the exhaust manifold. Therefore, it is necessary to introduce the Convective Augmentation Factor, as defined below.

$$CAF = \frac{Nu_{effective}}{Nu_{theoretical}} \quad (18)$$

This parameter should be applied to take into account the gas pulsations and sharp changes in the geometry. Based on previous research [4] the proper CAF value for exhaust gases is 2.5.

3.Description of the system

3.1. Exhaust system

The exhaust system collects the gas coming from the engine and treats it before the gas is released to the atmosphere. The exhaust system described in this thesis is composed of the manifold, turbocharger, catalytic converter and flexible pipe as illustrated in Figure 5.

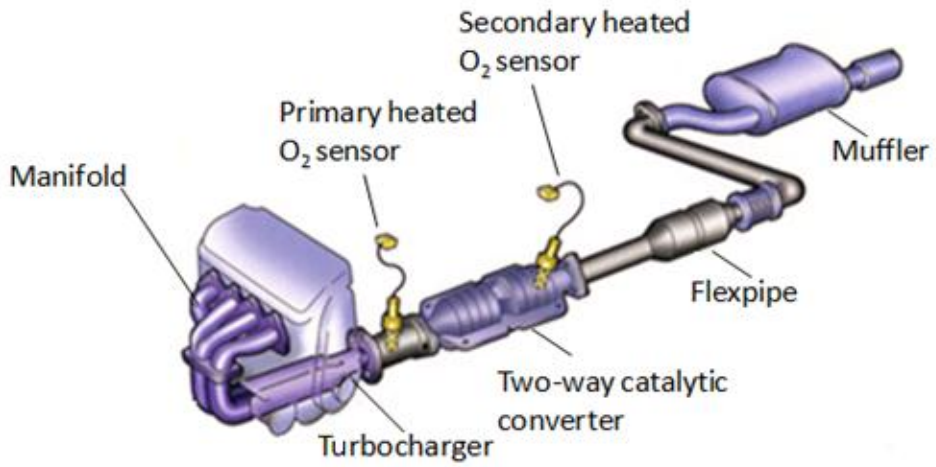

Figure 5. Exhaust system

It is important to notice that the exhaust system also incorporates a muffler and an exhaust gas recirculation system (EGR system). However, these parts are not further investigated in this thesis.

The exhaust gases leave the engine cylinder and are collected in the manifold. The gas streams flow inside the manifold and converge at the turbocharger. The turbocharger is divided into the turbine, center housing and compressor.

The exhaust gas flows through the turbine spinning blades leading to a pressure decrease in the exhaust gas. The combustion gases present enough pressure and temperature to produce a torque to drive the turbine to a very high speed. This rotation makes the compressor rotate as well since both contain the same shaft.

The compressor takes air from outside and forces it to pass through the volute where it is compressed. The compressor is made up of an impeller, a diffuser and volute housing. The compressor increases the density of intake air entering the combustion chamber.

The turbocharger geometry determines how the exhaust gas passes through the turbine and the compressor, influencing the overall turbocharger performance.

The two-way catalytic converter is applied to reduce the emission of combustion engines. The gas coming from the turbocharger consists of products of combustion and unburned hydrocarbons, which are hazardous for the environment. The catalytic converter presents two components: the diesel oxidation catalyst (DOC) and the diesel particulate filter (DPF).

The majority of the automotive catalytic converters contain a substrate made of metal or ceramic that supports the noble metal. The most common metals used as catalysts are platinum, palladium and rhodium [5]. The substrate consists of numerous channels with different geometries and an equivalent diameter of approximately 1mm. The design and model of the diesel oxidation catalyst depends on several parameters, some of them are stated below:

- Metal used as catalyst
- Diameter and length of the substrate (m)
- Cell density (cpsi)
- Washcoat thickness (m)
- Substrate material
- Geometry of cells

The exhaust gas passes through the substrate cells where oxidation reactions take place. The harmful compounds of the exhaust gases are converted into harmless compounds according to the following reactions [6].

$$CO + \frac{1}{2}O_2 \rightarrow CO_2 \;\; \Delta H = -283200 \; \frac{J}{mole}$$

$$C_3H_6 + \frac{9}{2}O_2 \rightarrow 3CO_2 + 3H_2O \; \Delta H = -1928000 \frac{J}{mole}$$

After the oxidation, the exhaust gas flows inside the diesel particulate filter that retains particles present in the gas. For this reason, the diesel particulate filter is also known as a particulate trap. The idea behind the use of DPF is to collect the engine-emitted soot and other particles on the walls of the device. The DPF is designed to regenerate itself. This means that when the amount of soot on the DPF walls reaches a certain value, the DPF is burned off. In most cases, the regeneration occurs when the exhaust temperature is higher than 600^{o}C.

The diesel particulate filter is characterized by the following parameters,

- Filter material
- Diameter and length of the filter (m)
- Cell density (cpsi)
- Geometry of cells
- Soot loading (kg/m^3)

- Length of end plugs (m)
- Soot pore diameter (m)
- Mass of ash loading (kg)

4. Method development

A method to predict the exhaust system temperature is described in this thesis. The inlet boundary condition is specified as one with a constant mass flow rate and with a representative temperature.

The method approximates the transient driving conditions with an equivalent steady-state condition. The method is validated against the results from the wind tunnel test carried out for the Hill Climbing Trailer Load (HCTR).

The method is developed by coupling CFD software (Fluent) with heat transfer analysis software (RadTherm). The external boundary conditions are obtained from 3-D CFD simulations carried out in Fluent 14.00 and the internal boundary conditions are derived from coupling with RadTherm 10.4.1. This coupling is necessary in order to model the advection of air temperature from the front to the rear of the vehicle which cannot be performed by only one-step import of convection coefficients from CFD.

One-dimensional models of internal flow in piping systems provide significant advantages over 3-D CFD by reducing both the model complexity and the computational time required to perform a simulation in some applications.

On one hand, Fluent solves the governing differential equations (Non-linear Navier-Stokes) and calculates heat transfer coefficients (h_{ext}) and film temperatures (T_{surf}) that are used as external boundary conditions in RadTherm. On the other hand, RadTherm performs an energy balance based on calculations of convection, conduction and radiation.

4.1. Mesh generation

The mesh used in RadTherm and in Fluent was provided and no further studies regarding the mesh are performed in this thesis since this is not the goal of the thesis.

4.2. Thermal Model Setup

The initial simulation uses estimated external boundary conditions (heat transfer coefficients and film temperatures) in order to provide an initial temperature profile of the exhaust system. This temperature profile is imported into the CFD software and used as a boundary condition. Multiply surface elements are grouped to form “patches” for radiative purposes to save computational effort. These RadTherm simulations are running on 8cpu cluster.

Before running the thermal model, it is necessary to define the environmental conditions. In this model the environment surrounding is modeled by the box environment. The bounding box environment is used for radiation exchange purposes. The temperature of the environment and the offset distance from the geometry to the walls of the box may be specified. A constant temperature of 70^{o}C and an offset distance of 1mm are used in this model.

4.3. CFD code

The CFD code used in this model is fluent, which solves the Navier-Stokes equations using a realizable k-epsilon turbulence model and enhanced wall functions. The air is modeled as an incompressible ideal gas. It is also considered that the density of the air only changes with the temperature.

The solver used in this model is the pressure-velocity coupling with the following spatial discretization.

- Second order discretization for pressure
- Second order upwind for the momentum
- First order upwind for the turbulent kinetic energy and turbulent dissipation rate.

The Fluent simulations are running on 240cpu cluster. These simulations provide film temperatures and convection coefficients to the thermal model, allowing the thermal model to recalculate the surface temperature.

4.4. CFD Coupling

The CFD coupling process is automated using a script developed by VCC. First, the thermal model is run using estimated boundary conditions to provide a temperature profile that is imported into the CFD code. The CFD model is run to convergence and new convection boundary conditions are exported to the thermal model. Finally, the thermal model is re-run providing a new temperature profile. This coupling loop continues five times more.

An overview of the modeling process is shown in Figure 6.

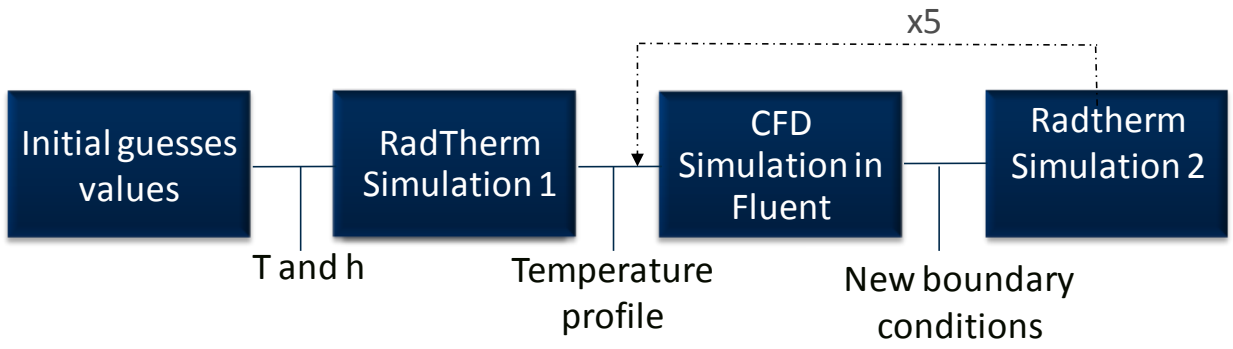

Figure 6. Coupling scheme. Heat transfer analysis software and CFD software.

First RadTherm is run using initial guesses for the heat transfer coefficient (h) and film temperatures (T) and a temperature profile is outputted. After that, Fluent uses this profile as a boundary condition to provide temperatures and heat transfer coefficients. Finally, these values are used as new boundary conditions in RadTherm.

This loop is repeated 5 times to ensure a converged solution, but this coupling would be optimized in future works. The estimated time for simulations is described as follows,

- Initial RadTherm model with initial guesses of h and T_{fluid} values takes around 50 minutes
- Roughly 4 hours are necessary to run a simulation in Fluent based on initial RadTherm values

- The time consumption during the looping simulations are 15 minutes in RadTherm and 35 minutes in fluent. The looping simulation uses the results from the previous coupling in order to speed up the process.

5. Thermal model development

5.1. Characterization of the manifold

There are five streams coming into the manifold one in each inlet and all of these streams converge into the turbocharger inlet. The first step to simulate the manifold is to define the value of the total mass flow rate and the inlet temperature of the exhaust gas in each manifold inlet. It is assumed that the mass flow is equal distributed in each pipe, which means that amount of exhaust gas coming into each manifold inlet is the same and it can be obtained dividing the total mass flow rate by the number of inlets.

The inlet gas temperature was estimated based on the temperature measured at the turbocharger inlet. As a first approximation, the inlet temperature of the exhaust gas was assumed the same in all the streams; however the results show that the temperature distribution at the inlet is not uniform, which means that each stream coming into the manifold presents a different temperature. The inlet temperature of the streams differs only by 10-20 ^{O}C and the left stream presents the highest temperature while the right stream has the lowest temperature.

Typical flow conditions in driving cases produce Re numbers higher than 2300 which means that the flow inside the manifold is turbulent. Even in cases where the Re is lower than 2300, the flow would remain turbulent because the exhaust valves and the pulsation effects do not favour the transition to the laminar region [3].

RadTherm is able to calculate the heat transfer rates bewteen the exhaust gas inside the manifold and the manifold inner wall by setting fluid streams inside the manifold geometry. Fluid streams are used in RadTherm to model a fluid inside pipes. When fluid streams are used in RadTherm, the heat transfer coefficients are automatically calculated by correlations based on flow rate and geometry. The mass flow rate and inlet tempertature of each stream should be set as input and also the inlet, outlet and direction of the streams.

In order to setup the streams in RadTherm it is necessary to split the geometry in several parts as it is shown in the Figure 7.

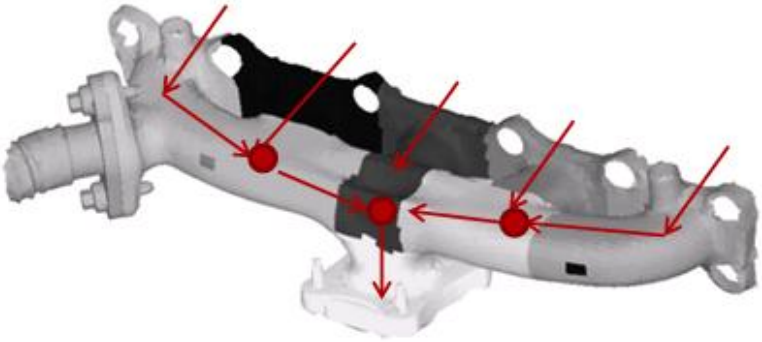

Figure 7. Manifold in RadTherm with five streams connected by advection links

Advection links are used in RadTherm to connect streams allowing transmitting the stream properties from one stream to another. When two streams are connected, the outlet properties of one stream are the same as the inlet properties of the other stream.

In this model advection links are required to connect upper streams with the stream coming into the turbocharger.

Convective effects of the stream are modeled by setting a convection boundary condition on each part bounding the fluid represented by different colors in Figure 7. The convection coefficient can be calculated using the correlations shown in Appendix A.

It is noteworthy that there is not any stream in the EGR. In this model the exhaust gas does not flow through the EGR since it was closed during the wind tunnel tests. In case that the EGR is open, another stream should be setup inside this part and a certain percent of the exhaust gas will be released through this pipe.

As it was explained in section 2.2., a Convective Augmentation Factor (CAF) equal to 2.5 is applied in the streams to take into account the gas pulsations and sharp changes in the geometry.

Table 1 shows the temperatures predicted by RadTherm using two different CAF values. The first column correspond to the data obtained in the tunnel test, the second column contains the temperatures predicted when a CAF equal one is applied and the last column corresponds to the temperature predicted when a CAF equal to 2.5 is used.

Table 1. CAF influence in the surface temperature prediction Results applying a CAF=1 and CAF =2.5.

Temperature (°C)	Tunnel test	CAF = 1	CAF =2.5
Exhaust manifold, right	537	479	528
Exhaust manifold, centre	590	566	594
Exhaust manifold, left	567	526	570
Exhaust manifold, left, at EGR pipe	441	367	445

As can be seen in Table1, the Convective Augmentation Factor presents a high influence in the surface temperatures. The simulation carried out with a CAF equal to 2.5 leads to a better prediction of surface temperature than using a CAF equal to 1 showing a maximum temperature deviation of three degrees. It is worth mentioning that these simulations were carried out by RadTherm without CDP coupling in order to reduce the computational time. The external convective coefficients and temperatures were imported from the same CFD data in all the simulations shown in Table 1.

5.2. Characterization of the turbocharger

One-dimensional (1D) models are commonly employed to study the performance of turbocharger engine. Much research shows that heat flows inside the turbocharger are non-negligible and they should be included in the turbocharger model.

The turbocharger is divided into compressor and turbine and these parts are connected through a bearing housing. Several researchers [7], [8] have shown that heat transfer is not small during the compression and the expansion; therefore, a 1-D heat transfer model is developed and validated against the experimental measurements. A simply scheme of energy changes can be seen in the Figure 8.

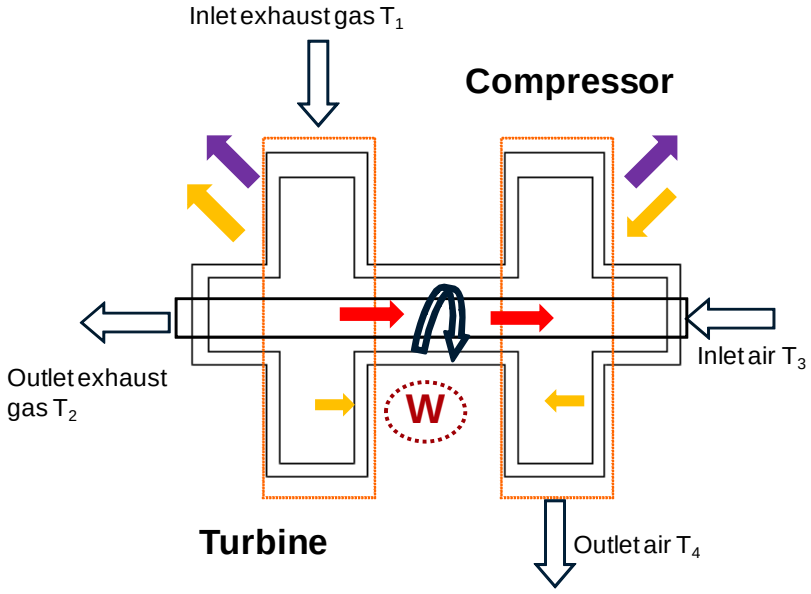

Figure 8. Heat transfer model of the turbocharger. Radiation, convection and conduction heat fluxes.

As it can be seen in Figure 8 there are radiation and free convection between the turbine, the bearing housing and compressor with the environment. The compressor temperature is lower than the bearing casing temperature while the turbine temperature is higher than the bearing casing which leads to a conduction heat transfer between these parts. There is also forced convection between the exhaust gas and the turbine surface due to the gradient temperature between them which leads to a decrease in the outlet gas temperature. Inside the turbine the heat is conducted through the wall and dissipated to the environment by radiation and free convection.

A similar reasoning can be applied for the compressor but in that case, the outlet air temperature in the compressor increases due to the fact that the compressor presents a higher surface temperature than within the compressor.

A more detailed description of the compressor and turbine is explained in the following subsections**.**

Characterization of the compressor

The cold air from the environment passes through the inlet pipe and comes into the compressor volute. The air passes through the spinning blades describing an elliptic movement inside the volute. The compression of the air leads to an energy absorption in the form of work that warms up the air. After the compression, the warm air leaves the turbine through the outlet pipe.

As it was mentioned before the air describes an elliptical movement inside the compressor that cannot be modeled by RadTherm. Therefore, the fluid stream inside the volute should be modeled as a fluid node with an imposed heat equal to the work that it is introduced during the air compression. A fluid node represents the bulk properties of a specific volume of liquid. Fluid nodes can be connected to another parts through advection links. It can be seen in Figure 9 how the turbo is modeled by RadTherm.

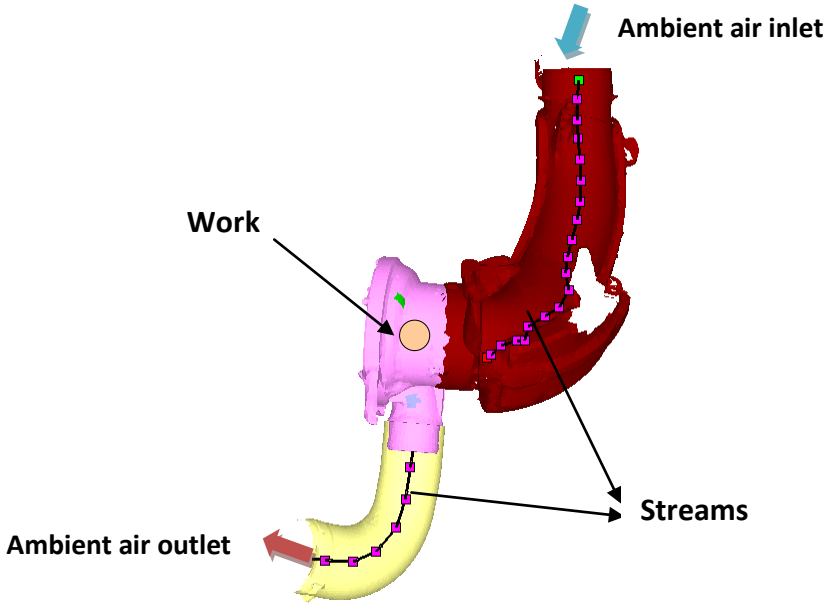

Figure 9. Compressor modeled by a fluid node, inlet and outlet streams. Compressor work imposed on the fluid node.

The compressor is modeled using an inlet stream, a fluid node inside the volute and an outlet stream.

In order to setup the inlet and outlet streams in RadTherm it is necessary to define the mass flow rate and inlet temperature. Once the streams are setup in the model, RadTherm calculates the heat transfer coefficients to obtain the convection heat rates.

The energy of the air inside changes due to the compression and according to the first law of thermodynamics, this change of energy is equal to the sum of the work and the heat transfer. In this case, the amount of work released during the compression should be calculated and imposed in the fluid node; while the heat transfer rates can be modeled and calculated by RadTherm.

As explained before the heat losses in the compressor cannot be neglected and the air properties at the compressor inner and outer surfaces should be known to calculate the compressor work.

In order to calculate this value it is important to notice that the isentropic efficiency can be defined in two different ways, depending whether or not heat losses are considered. Theses efficiencies are divided into non-adiabatic (η_{c_O}) and adiabatic (η_{c_R}) [7].

$$\eta_{c_O} = \frac{\dot{m} \cdot \Delta h_{c_{is}}}{\dot{m} \cdot \Delta h_c} = \frac{\dot{m} \cdot \Delta h_{c_{is}}}{P_c} \quad (19)$$

$$\eta_{c_R} = \frac{\dot{m} \cdot \Delta h_{c_{is}}}{\dot{m} \cdot \Delta h_c - \dot{Q}} = \frac{\dot{m} \cdot \Delta h_{c_{is}}}{\dot{W}} \quad (20)$$

Figure 10 shows the efficiency curves for a compressor using different inlet temperatures.

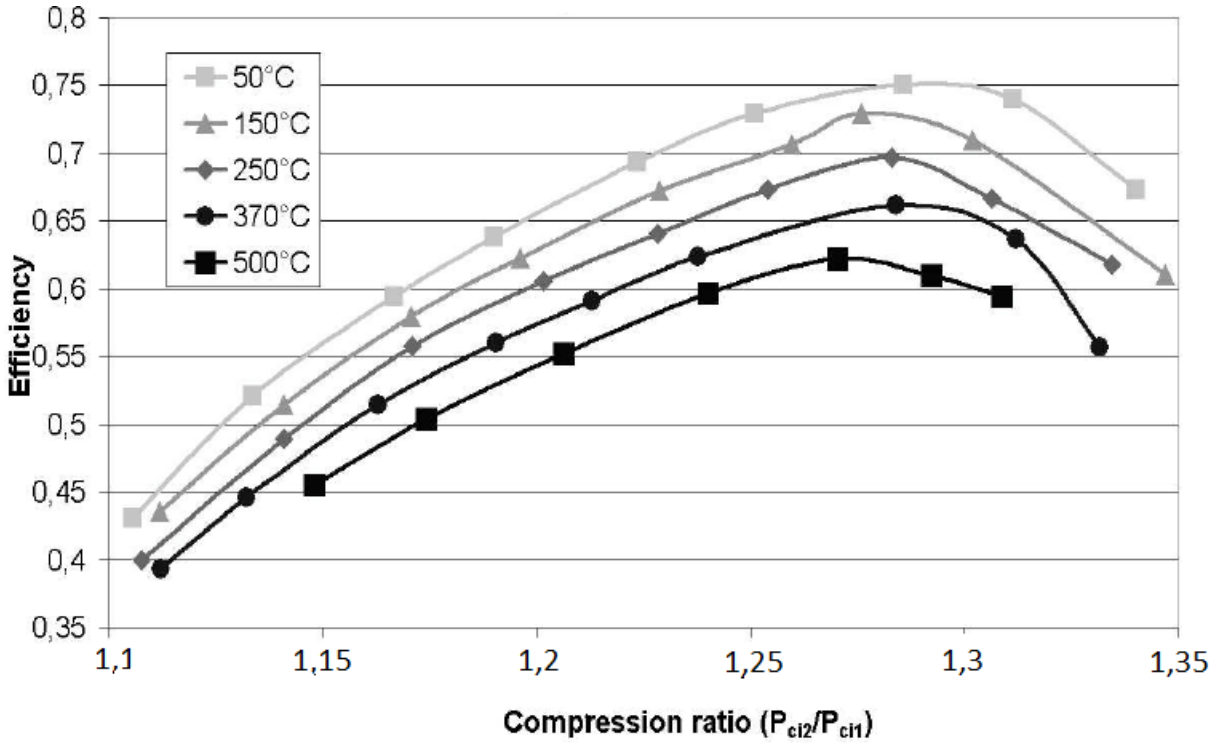

Figure 10. Apparent compressor efficiency for various turbine inlet temperatures [8]

The adiabatic efficiency is a parameter that only depends on the compressor geometry and the pressure ratio and it does not depend on the inlet air temperature. This means that this efficiency will only depend on the pressure ratio and the compressor geometry. However, the Figure 10 shows different curves depending on the inlet turbine temperature which means that the heat transfer in the turbocharger cannot be neglected.

In order to get the real compressor efficiency it is necessary to reduce the heat losses to zero. If the heat losses tend to zero, the energy change in the air only is transferred into work.

In order to decrease the heat losses, it is necessary to carry out experiments with similar temperature values of the compressor inlet temperature, compressor surface temperature and environmental

temperature. If the temperature gradient tends to zero, the heat losses will tend to zero too so the compressor power will be the same as the work. This experiment can be done several times varying only the pressure ratio in order to get the efficiency curve. This curve can be used to calculate the work under different inlet air temperature since this curve only depends on the pressure ratio and the compressor geometry.

As was explained above, it is necessary to obtain the compressor work in order to impose it on the fluid node inside both the compressor and turbine. For this case, the work was given by the Powertrain Department at VCC due to the complexity of the methodology required to calculate the work. The Powertrain department performed experiments minimizing the effects of heat transfer on the compressor efficiency. These experiments were carried out running the turbine at room temperature to eliminate the primary heat source. Moreover, the temperature compressor housing was controlled by conditioning cooling water and oil in order to match the outlet air temperature of the compressor.

Once the work is defined, it is necessary to calculate the heat transfer coefficients in each part of the compressor: inlet, volute and outlet to obtain the heat transfer rates in the turbocharger.

Heat transfer coefficient at the inlet and outlet of the compressor

The heat transfer coefficients in the compressor inlet and outlet are calculated by RadTherm using the correlations described in Appendix A (equations A1 to A4).

Heat transfer coefficient at the compressor volute

Using correlations to calculate the Nusselt number inside the volute will introduce high level of uncertainty due to the complex geometry and flow inside the volute. Therefore, simulations in STAR-CCM+ are carried out by the PowerTrain department at VCC to estimate the heat transfer coefficient inside the volute. The simulations done by the PowerTrain department presents a higher mass flow rate than the model described in this thesis; therefore, a correction of the Nusselt number should be applied. As it was explained in the Section 4, the Nusselt number can be described as follows,

$$Nu = a \cdot \mathrm{Re}^{b}\ \mathrm{Pr}^{c} \quad (21)$$

Where a, b and c only depends on the fluid properties and compressor geometry so the only parameter affected by the mass flow rate is the Reynolds number. If the model described in this thesis is called Case 1 and the case simulated by the Powertrain department is called Case 2, the relation between Nusselt numbers of both cases is shown in equation 22.

$$\frac{Nu_1}{Nu_2} = \left(\frac{m_1}{m_2}\right)^{b} \quad (22)$$

The heat transfer coefficient is proportional to the Nu number so the heat transfer coefficient inside the volute (h_1) is calculated as follows,

$$\frac{h_1}{h_2} = \left(\frac{\dot{m}_1}{\dot{m}_2}\right)^{b} \quad (23)$$

It is noteworthy that the exponent b presents a typical value around 0.8 for air [2].

The heat transfer coefficients obtained are shown in Table 2.

Table 2. Heat transfer coefficients inside the compressor

Turbocharger component	Heat transfer coefficient (W/m2K)
Compressor inlet	[85-95]
Compressor volute	[585-595]
Compressor outlet	[185-195]

Characterization of the turbine

The methodology used for the turbine is quite similar to the one used for the compressor described in the previous section

The exhaust gas coming from the manifold converges into the inlet turbine and is expanded inside the turbine. The expansion of the exhaust gas leads to a release of energy in the form of work.

As it was mentioned in the previous subsection, the gas describes an elliptical movement inside the turbine that cannot be modeled by RadTherm. Therefore, it is necessary to setup a fluid node inside the volute. It can be seen in Figure 11 how the turbo is modeled by RadTherm.

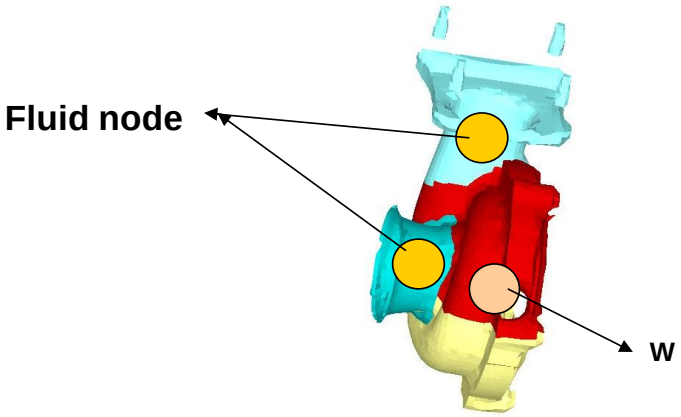

Figure 11. Turbine modeled in RadTherm. Fluid nodes at the inlet and outlet. Fluid node with imposed heat inside the turbine.

The compressor shaft is the same as the turbine shaft therefore the compressor work will be the same as the turbine work. In other words, the imposed heat that is applied on the compressor as a positive heat is also imposed on the turbine as negative heat.

Once the work is defined, it is necessary to evaluate the heat transfer between the gas and the inner wall.

First, the turbine is divided in several parts: inlet, volute and outlet. A fluid node is set in each part to evaluate the heat transfer within each part. The next step corresponds to calculate the heat transfer coefficients in each fluid node. The turbine inlet and outlet can be modeled as pipes and the Nu number can be calculated using the correlations of flow inside circular ducts (Gnielinksi (1976)). The heat

transfer coefficient inside the volute is calculated in the same way as the heat transfer coefficient in the compressor.

Heat transfer coefficient at the turbine volute

The heat transfer coefficient at the turbine volute is obtained in the same way as the compressor heat transfer coefficient. The only difference regarding the relation shown in equation 23 is that the exhaust gas presents different properties than the ambient air so the constant b is not 0.8.

According to [9], [10] and [11] for engine exhaust gas the exponent b presents a typically value around 0.75.

Heat transfer coefficient at the inlet and outlet of the turbine

According to equation 8 shown in the section 4, the turbulent hydrodynamic entry length is higher than the half-width of the duct, which means that the flow is non-fully developed. Therefore, the correlations provided by Gnielinski (1976) and Kakaç et al. (1987), shown in Appendix A, are used to calculate the convective coefficients.

Since the correlations applied correspond to an undeveloped flow, the use of the CAF may not be necessary. Part of the reasoning behind the use of the CAF in the streams is that the pulsations prevent the flow from fully developing and this effect is already taken into account in the correlations.

Even though these correlations estimate properly the heat transfer coefficient, it is recommendable to use the heat transfer from the CCM+ simulations due to the complexity of the flow inside the turbine. The heat transfer coefficients used in this model are obtained in the same way as the turbine volute.

Table 3 shows a summary of the heat transfer coefficients inside the turbine.

Table 3.Heat transfer coefficients inside the turbine

Turbocharger component	Heat transfer coefficient (W/m^2K)	
	Correlations	Powertrain Department
Turbine inlet	[260-270]	[625-635]
Turbine volute	[200-210]	[750-760]
Turbine cone out	[345-3555]	[565-575]
Turbine clamp	[185-195]	[450-460]

5.3. Characterization of the catalytic converter

The catalytic converter can be divided into two components: the diesel oxidation catalyst (DOC) and the diesel particulate filter (DPF). The catalytic used in diesel engines is usually a two ways catalytic illustrated in Figure 12.

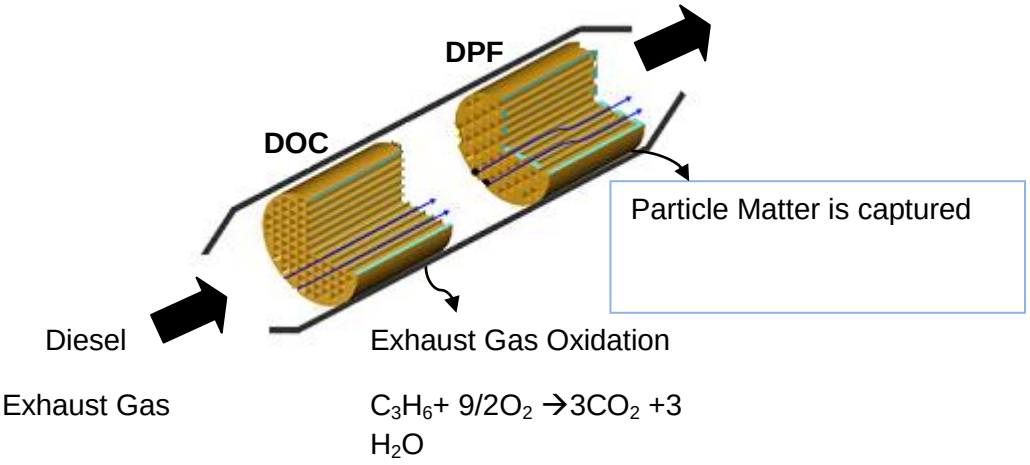

Figure 12. Catalytic converter. Diesel Oxidation Catalyst (DOC) and Diesel Particulate Filter (DPF)

In order to evaluate the heat transfer phenomena in the catalytic converter, the catalytic converter is divided in several parts, each evaluated in a different fashion. The catalytic is divided into catalytic inlet, DOC, catalytic middle, DPF and catalytic cone out as shown in Figure 13. A fluid node is setup in each part to evaluate the heat transfer in each part.

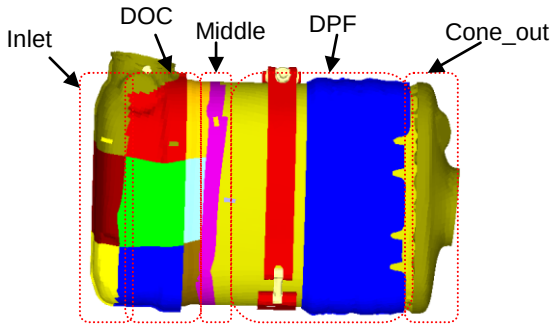

Figure 13. Catalytic parts. Inlet, DOC, Middle, DPF and Cone_out

It is noteworthy that the exhaust gas distribution inside the catalytic is not uniform. The exhaust gas resents preferential paths that contribute to a non-uniform flow distribution inside the catalytic.

In collaboration with the Powertrain department, simulations of the VED5 CCDPF FWD catalytic converter were carried out in STAR-CCM+ to obtain the uniformity index inside the catalytic converter. Results from these simulations are shown in the Appendix B.

Table 4 contains the DOC and the DPF uniformity index obtained from the STAR-CCM+ simulations.

Table 4. Uniformity Index of the DOC and DPF

Catalytic converter component	Uniformity index
DOC	0.8
DPF	0.97

According to Figure 31 in the Appendix B and Table 4, it is reasonable to affirm that the flow distribution in the catalytic inlet and inside the DOC is not uniform. When the exhaust gas leaves the DOC, the flow is uniformly dispersed and the flow distribution in the catalytic middle, inside the DPF and in the catalytic cone out is considered homogeneous.

It is difficult to know and simulate the exactly distribution of the gas flow. As a first approximation, it is reasonable to divide the catalytic inlet and DOC in three parts based on the three different flow paths observed in Figure 30 in the Appendix B.

In order to model the gas flow distribution, the inlet stream is split in three fluid nodes as it can be seen in figure 14.

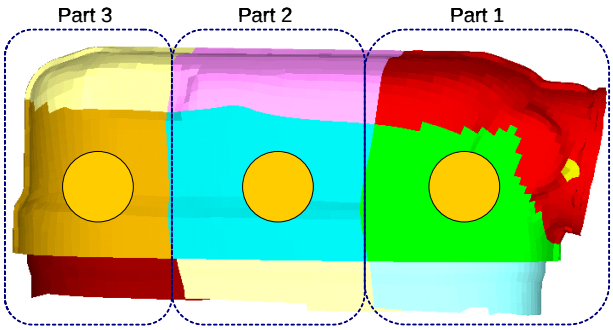

Figure 14. Catalytic fluid nodes inside each part.

Figure 30 in Appendix B shows that most of the gas flows through the middle of the substrate and only a few percent of the flow pass through the first part. Therefore, it is assumed the following gas distribution:

- Part 1. 0% of the gas stream
- Part 2. 60% of the gas stream
- Part 3. 40% of the gas stream

Characterization of the catalytic inlet

As it was explained before, the gas flow distribution at the catalytic inlet is not uniform so that the catalytic inlet is split in three different parts and a fluid node is setup inside each part to individually

evaluate the heat transfer between the gas stream and the inner catalytic wall. The fluid nodes are connected with the upstream nodes applying the following relations,

$$\dot{m}_{catalytic\_inlet\_node\_1} = \dot{m}_{tutbo\_outlet}$$
$$\dot{m}_{catalytic\_inlet\_node\_2} = (1-x_1)\cdot \dot{m}_{catalytic\_inlet\_node\_1} \qquad (24)$$
$$\dot{m}_{catalytic\_inlet\_node\_3} = x_3 \cdot \dot{m}_{total} = \frac{x_3}{(1-x_1)} \cdot \dot{m}_{catalytic\_inlet\_node\_2}$$

where x_i is the percent of the mass flow rate coming into each part.

Once the fluid nodes are defined in RadTherm, it is necessary to define the heat transfer coefficient in each part in order to calculate the convection heat transfer between the exhaust gas and the inner wall. Due to the complex geometry and the pulsating nature of the exhaust gas, the flow is not fully developed and correlations for internal non developed flow should be used to calculate the Nu number in the catalytic inlet.

As explained before when correlations for non-developed flow are applied, the CAF may not be necessary.

Table 5 shows the heat transfer coefficient values for the catalytic inlet parts.

Table 5.Heat transfer coefficients inside the catalytic inlet

Catalytic inlet	Heat transfer coefficient (W/m2K)
Part 1	[310-320]
Part 2	[345-355]
Part 3	[250-260]

Characterization of the DOC

The diesel oxidation catalyst (DOC) contains a brick and a substrate. The brick is the external part of the DOC, which is surrounded by a heat shield. The DOC substrate is defined as a stainless steel matrix with several cells where the exhaust gas passes through.

The exhaust gas flows inside the substrate cells which leads to a convection heat transfer between the gas and the substrate. The exhaust gas presents a higher temperature than the substrate so the heat is transferring from the exhaust gas to the substrate surface increasing in the catalytic converter surface temperature.

The substrate is in contact with the backside of the catalytic brick. This causes heat transfer via conduction through the contact area between the substrate and the backside of the brick. The heat transfer that occurs inside the DOC can be summarized by the following components:

- Forced convection heat transfer between the exhaust gas and the substrate cells.
- Conduction between the outside wall of the substrate and the inner wall of the catalytic brick.

It is noteworthy that oxidation reactions occur inside the substrate and a certain amount of energy is released during this process. Consequently, the temperature of the exhaust gas will increase.

Moreover, it is important to take into account the pressure drop in the substrate due to the small dimensions of the cells. The friction with the inner cell walls will decrease the energy of the exhaust gas when gas flows inside the cells.

Due to the complexity of the DOC substrate geometry, this substrate is simulated in RadTherm as a lumped capacitance. The calculated lumped capacitance part has a single node associated with it and is shown as being available when a part is created without geometry. Temperature gradients within the part are assumed to be negligible. This lumped capacitance part may be connected to the gas flowing inside and to the catalytic brick via conduction.

The diesel oxidation catalyst model is separated in inside part, middle part and external part.

INSIDE PART: Exhaust gas flow inside the DOC substrate

In this subsection the modeling of the exhaust flow inside the cells is described.

In order to model the substrate as a lumped capacitance in RadhTherm, it is necessary to define the volume and the area of this lumped. The volume of the substrate represents the solid volume of the substrate and the area corresponds to wetted area, which is defined as the total area in contact with the fluid.

The first step in modeling the substrate is to calculate the volume (or mass) and the area of the lumped capacitance used in RadTherm. The geometry and properties of the substrate are detailed in the Appendix C.

The area of the lumped capacitance depends on the geometry of the cells that present a trapezoidal cross-sectional area as shown in Figure 15.

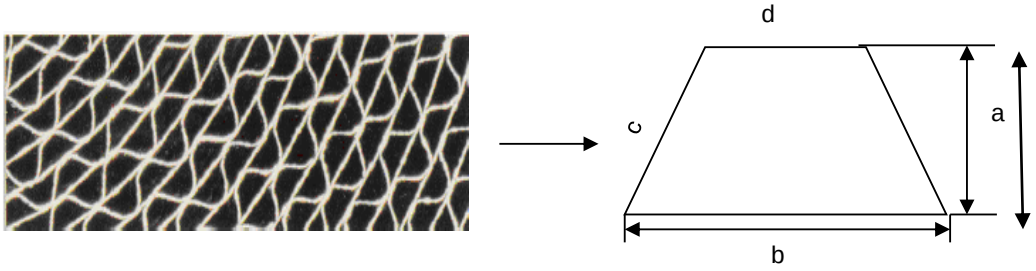

Figure 15. Diesel Oxidation Catalyst Substrate Geometry

Using the data from the supplier and applying geometrical relations, the internal dimensions of the cell, the internal perimeter and cross-sectional area of the cell are obtained. This calculation is described in more detail in the Appendix C.

Once the cell geometry is well defined, it is easy to calculate the lumped area as the total area of the substrate in contact with the exhaust gas.

$$A_{wetted} = P_{internal} \cdot L_{subtrate} \quad (25)$$

$$A_{lumped} = A_{wetted} \cdot n_{cells} \quad (26)$$

The mass of the lumped is equal to the total mass of the substrate that it is given by the supplier

As explained in the previous section, the flow distribution inside the DOC is not uniform so the DOC is divided into three parts,

- The substrate is modeled by three lumped capacitances with the same dimensions.
- The exhaust gas stream is divided in three nodes connected with the upstream nodes.

The properties of each lumped capacitance are obtained under the assumption that the lumped capacitances have the same area, the same mass and equal number of cells.

$$A_{lumped_i} = \frac{A_{lumped_{total}}}{3} \qquad m_{lumped} = \frac{m_{lumped_{total}}}{3} \quad (27)$$

The second step is to define the gas fluid nodes in RadTherm by connecting them with the upstream nodes. Even though the exhaust gas mass flow rate changes due to the oxidation reactions that occur inside the DOC, a constant gas mass flow rate through the whole system is assumed in this method. The follow relations are used to define the mass flow rate in each node.

$$\dot{m}_{DOC\_node\_1} = x_1 \cdot \dot{m}_{catalytic\_inlet\_node\_1}$$

$$\dot{m}_{DOC\_node\_2} = \frac{x_2}{1 - x_1} \cdot \dot{m}_{catalytic\_inlet\_node\_2} \quad (28)$$

$$\dot{m}_{DOC\_node\_3} = \dot{m}_{catalytic\_inlet\_node\_3}$$

where x_i is the percent of the mass flow rate of each node.

Having reached this point, it is necessary to create advection links between the lumped capacitances and the fluid nodes by defining the heat transfer coefficient between the gas and the cells.

The Reynolds number obtained is lower than 2300 that means that the flow inside the substrate is laminar and the correlation of Hornbeck (1965) can be applied.

Based on the Nusselt number obtained, the heat transfer coefficient for each lumped capacitance is obtained applying the equation (29)

$$h = \frac{Nu \cdot k}{D_h} \quad (29)$$

The exhaust gas passes through the substrate cells where the oxidation of compounds into other compound less dangerous takes place. Platinum (Pt) is located in the cells surfaces [5] and it acts as catalyst for the reactions described in section 3.

All the reactions that occur inside the substrate are exothermic, which means that a certain amount of heat is generated. The heat released during the reaction will warm up the exhaust gas inside the substrate so that the surface temperature of the catalytic converter will also be increased.

For this model, only the value of the energy released during the reactions is important. This reaction heat depends on the gas flow rate and the concentration of carbon monoxide [CO] and hydrocarbons [HC] in the exhaust gas at the inlet of the substrate. The concentration of the CO and HC were measured experimentally by the After treatment department at VCC.

The total heat released during the reactions is calculated using the equation (30).

$$Q_{reaction} = moles_{C_3H_6} \cdot \Delta H_{reaction} + moles_{C_3H_6} \cdot \Delta H_{reaction} \quad (30)$$

The number of moles are calculated based on the concentration given by the After treatment department as explained in the Appendix C. It is also important to consider the heat losses due to the friction inside the substrate. The exhaust gas flows inside the substrate through small channels that leads to a significant pressure drop between the substrate inlet and outlet. The pressure drop was given by the supplier to the Powertrain Department. Based on this pressure drop, the dissipated energy is obtained as follows,

$$Heat\_losses = \dot{V}_{exhaust\_gas} \cdot \Delta P_{substrate} \quad (31)$$

where $\dot{V}_{exhaust\_gas}$ is the volumetric flow rate. The other losses due to the inlet channel contraction and outlet channel expansion can be neglected [12].

The heat released during the reactions is considered as a heat source while the pressure drop is modeled as a heat sink. Therefore, the reaction heat is defined as a positive imposed heat on the lumped capacitance while the heat losses are defined as negative imposed heat pn the node.

Due to the fact that the reaction heat and the heat losses depend on the mass flow rate, it is not realistic to set the same imposed heat in all the lumped capacitances and fluid nodes. It is reasonable to set a higher imposed heat in the part of the DOC where the mass flow rate is higher.

The imposed heat in each lumped and fluid node is estimated by the following relations

$$Q_{lumped\_i} = x_i \cdot Q_{reaction} \quad (32)$$

$$Heat\_losses_{node\_i} = x_i \cdot Total\_heat\_losses \quad (33)$$

where x_i is the percent of the mass flow rate of each part.

A summary of the lumped capacitance parameters and the imposed heat in each part is illustrated in Table 6.

Table 6.Lumped capacitances and imposed heats in each part of the DOC

Parts inside the DOC	Lumped area (mm^2)	Lumped mass (kg)	Imposed heat (W)	
			Lumped	Fluid node
Part 1	855060	0.923	0	0
Part 2	855060	0.923	250	-250
Part 3	855060	0.923	200	150

Middle Part: Conduction heat transfer between the outside of the substrate and the inner wall of the brick

In the reality, the outside part of the substrate is not in plenty contact with the inner brick wall; however, it is assumed that both parts are in fully contact and only conduction heat transfer takes place in order to simplify the model.

As it was explained before, the substrate in RadTherm is not simulated as a solid that's why RadTherm cannot calculate the heat transfer transferred from the substrate to the brick through the area in contact. Nevertheless, RadTherm is able to calculate the convection heat transfer between a lumped capacitance and a solid; therefore, the heat transfer should be simulated as convection. Interstitial heat transfer occurs between two surfaces due to the fact that they can never present a perfect thermal contact.

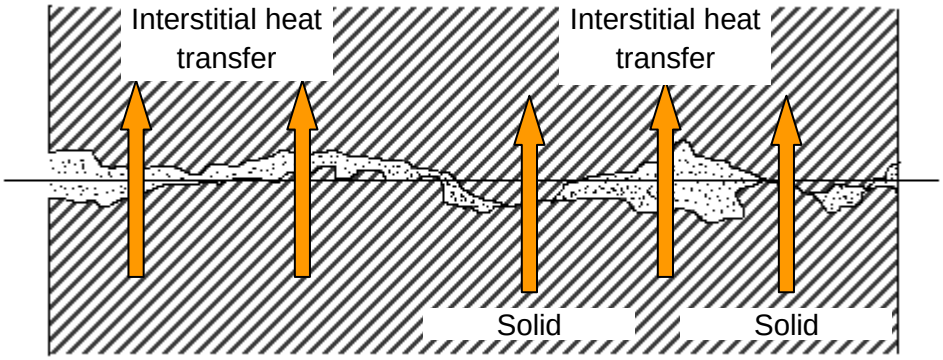

Figure 16. Heat transfer between two surfaces in fully contact

Contact surface can be treated as a surface with and internal conductance, h_c, (W/m^2K). This conductance is obtained as the inverse of the contact resistance and it depends on the surface finish, on the material, on the pressure, on the substance in the interstitial spaces and on the temperature. [13].

According to the electrical analogy shown in Figure 17, the heat transfer coefficient defined in RadTherm is equal to the internal conductance, h_c.

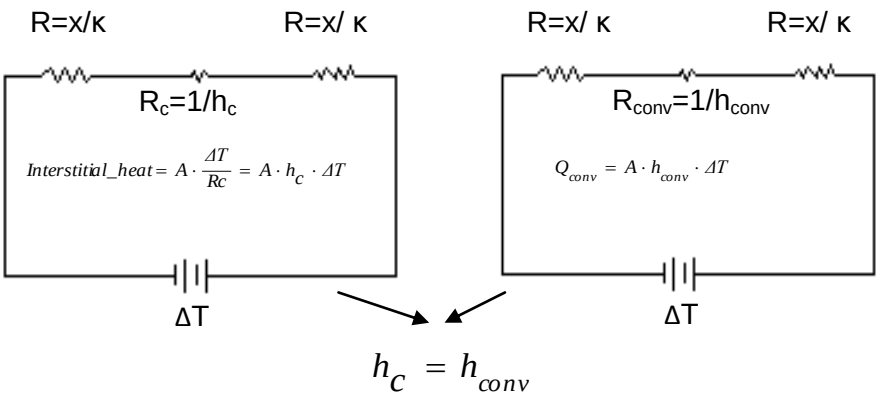

Figure 17. Electrical analogy. Comparison of the convection and conduction heat transferred based on the same temperature difference.

The brick and the substrate are both made of stainless steel and the conductance of stainless steel varies from 2000-3700 (W/m^2K) according to the bibliography [13]

Based on the results from the sensitivity analysis in section 5 the contact resistance does not present a great influence in the surface temperature, which means that any value from 2000 to 3700 can be set as conductance. The value chosen for this model is 2000 (W/m^2K).

External part: Conduction heat transfer between outside wall of the brick and heat shield

The last step of the DOC characterization is modeling the heat shield that surrounds the DOC brick. The heat shield is made of stainless steel and an isolation mat is situated between the back side of the shield and the front side of the brick. Therefore, the heat shield is modeled in RadTherm as a two-layer component with isolation on the backside and stainless steel on the front side.

The heat is transferred from the brick to the heat shield by conduction so a thermal link is created between the front side of the brick and the back side of the heat shield. RadTherm will not calculate convection heat and radiation heat when a thermal link is defined between two parts.

In order to create a thermal link it is necessary to define the contact resistance between parts. Based on the results from the sensitivity analysis in section 7.3 the contact resistance is not an influent value so that a default value (10000 W/m^2K) is applied in this case.

Figure 18 illustrates how the DOC is modeled in RadTherm.

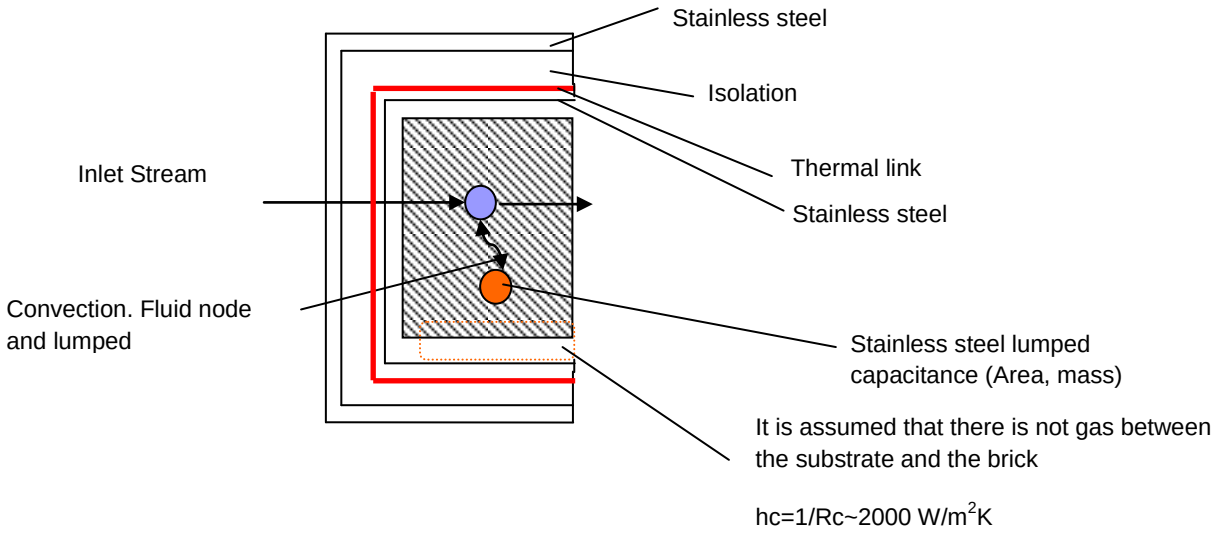

Figure 18. DOC modeled in RadTherm

A summary of the heat transfer coefficients in this section are shown in Table 7.

Table 7. DOC heat transfer coefficients

Diesel oxidation catalyst	Heat transfer coefficient (W/m^{2}K)		
Inside part	**Part 1**	**Part 2**	**Part 3**
	[215-225]	[235-245]	[230-240]
Middle part	2000		
External part	10000		

Characterization of the catalytic part between the DOC and the DPF

After the oxidation of some compounds, the exhaust gas is filtered in the diesel particulate filter (DPF) before leaving the catalytic converter. There is a small part of the catalytic converter between the DOC and the DPF that is called catalytic middle part in this model.

The exhaust gas distribution inside this part is uniform and the stream is modeled as a fluid node connected with the upstream nodes as follows,

$$\dot{m}_{catalytic\_middle\_node} = \dot{m}_{DOC\_node\_1} + \dot{m}_{DOC\_node\_2} + \dot{m}_{DOC\_node\_3} \quad (34)$$

The heat transfer coefficient inside this part is calculated using the same correlation (Gnielinksi (1976)) applied in the catalytic inlet. According to this correlation, the heat transfer coefficient is 150 W/m^{2}K.

Characterization of the DPF

The diesel particulate filter (DPF) is divided into brick and the filter. The filter is made of several ceramic cells designed to remove the diesel particle matter or soot from the exhaust gas when the gas passes through these cells. The brick is the external part of the DPF which is surrounded by a heat shield.

The diesel particulate filter is modeled following the same methodology applied to the diesel oxidation catalyst.

According to the results from the Powertrain Department, the gas flow distribution inside the DPF is uniform so only one lumped capacitance and one fluid node are defined in RadTherm.

The heat transfer exchanges that take place inside the DPF are summarized in following points,

- Forced convection heat transfer between the exhaust gas and the substrate cells.
- Conduction between the outside wall of the substrate and the inner wall of the catalytic brick.

It is important to notice that in this model there is not considered regeneration in the DPF because this process did not occur during the tunnel test used in the validation. Therefore, only imposed heat in the DPF is due to the pressure drop between the inlet and the outlet of the DPF.

During the filtration, particles are retained in the DPF leading to a cake formation in the top of the filter. In addition, particles can get lodged inside the channels, causing disruptions in the gas flow. For these reasons, the pressure drop inside the DPF cannot be neglected in the model.

In the same way as the diesel oxidation catalyst, the diesel particulate filter is divided into inside part, middle part and external part.

Inside 1: Exhaust gas flow inside the filter

As explained before, the first step to characterize the filter is to calculate the area and the volume of the lumped capacitance. In order to calculate these parameters, a methodology similar to the previous one is applied.

The filter embedded in the system is a ceramic filter with square cells made of Aluminum Titanate ($TiAl_2O_5$). A diesel filter usually looks like Figure 19 where the black rectangles correspond to the filter plug.

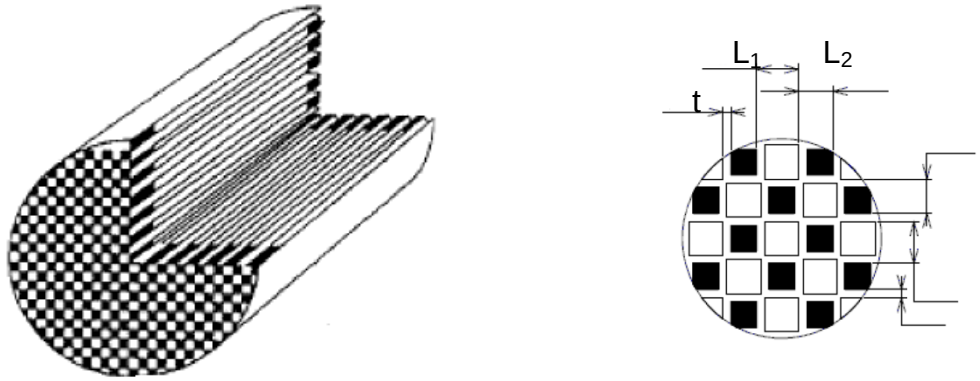

Figure 19. Diesel Particulate Filter scheme

Using the data from the supplier and applying geometrical relations it is possible to obtain the internal dimensions of the cell, the internal perimeter and cross-sectional area of the cell as described in Appendix C.

According to equation (35) the volume of the lumped capacitance is equal to the total solid cylinder minus the volume of the cell.

$$V_{lumped} = V_{solid\_filter} - V_{cells} \quad (35)$$

The second step is to define the gas fluid nodes in RadTherm by connecting them with the node in the middle of the catalytic converter.

Once the lumped and the node are defined, it is necessary to calculate the heat transfer coefficient. The velocity of the exhaust gas inside the filter should be carefully calculated since this velocity depends on the mass flow rate inside the cells. The trajectory of the gas inside the filter is represented in Figure 20

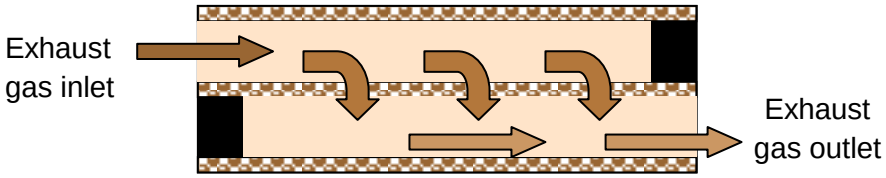

Figure 20. DPF channels

According to Figure 20, the exhaust gas is filtered when it passes through the wall of the cell due to the fact that these cells are made of a porous material. The mass flow rate in each cell can be calculated as follows.

$$\dot{m}_{DPF\_cell} = \frac{\dot{m}_{total}}{0.5 \cdot n_{cells}} \quad (36)$$

The Reynolds number obtained is lower than 2300 that means that the flow inside the filter is laminar. The Shah and Lond (1978) correlation for a laminar, hydrodynamically and thermally fully developed flow in a rectangular duct is used to calculate the Nusselt number inside the DPF cells as described in Appendix A.(Equation A9).

The next step is to evaluate the amount of heat losses inside the DPF. The pressure drop was given by the supplier. Multiplying the measured pressure drop by the volumetric flow rate, the energy dissipated in the DPF is obtained. Finally, this energy is defined as a negative imposed heat on the fluid node inside the DPF.

The lumped capacitance dimensions and the imposed heat in the fluid node is summarize in the Table 8.

Table 8.Lumped capacitance dimensions and imposed heat in the DPF node

Lumped volume (cm^3)	Lumped Area (mm^2)	Imposed heat in the fluid node(W)
1105	2893140	-2000

Middle Part: Conduction heat transfer between the outside of the filter and the inner wall of the brick

The heat is transferred through the area in contact with the brick. An isolation mat surrounds the filter in order to reduce the surface temperature of the brick.

According to the previous section, the conduction heat transfer is modeled as convection heat using a heat transfer coefficient equal to the conductance.

Based on the results from the sensitivity analysis described in section 7.5, the contact resistance is not an influent value so that a default value (10000 W/m^2K) is used in this model.

External part: Conduction heat transfer between outside wall of the brick and heat shield

As well as in the DOC, a heat shield surrounds the DPF brick and a thermal link is defined between these parts as it was explained in the previous subsection.

Figure 21 illustrates how the DPF is modeled in RadTherm.

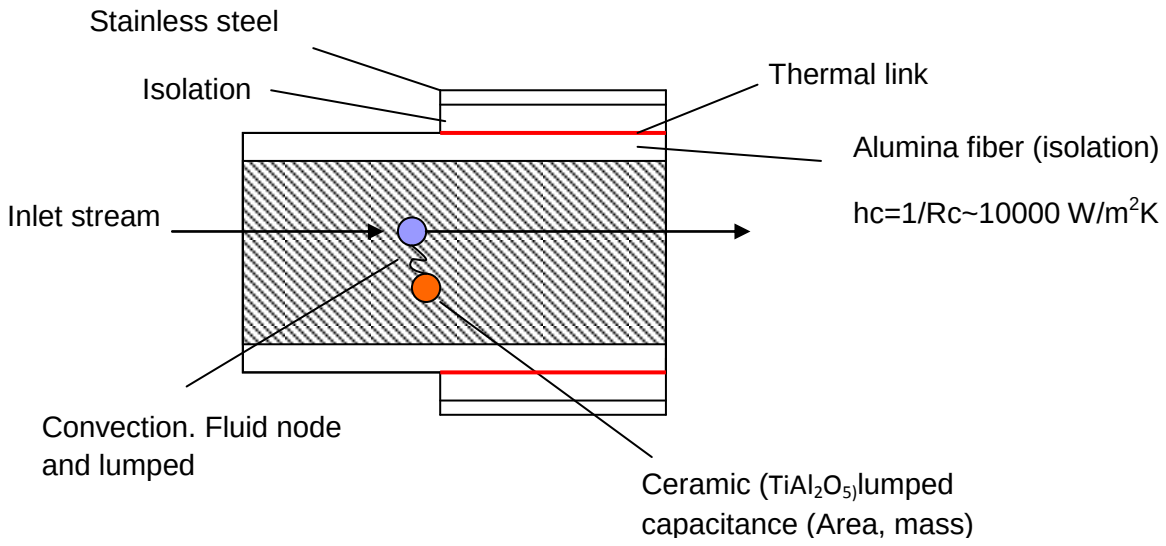

Figure 21. Diesel Particulate Filter modeled in RadTherm

A summary of the heat transfer coefficients in this section are shown in Table 9.

Table 9.Heat transfer coefficients in the DPF

Diesel particulate filter	Heat transfer coefficient (W/m2K)
Inside part	[125-135]
Middle part	10000
External part	10000

Characterization of the catalytic outlet cone

After the DPF, the exhaust gas flows through the catalytic cone before leaving the catalytic converter. This stream is simulated as a fluid node connected with the node inside the DPF and the heat transfer coefficient is calculated using Gnielinksi (1976) correlation According to this correlation; the heat transfer coefficient is 160 W/m^2K.

5.4. Characterization of the exhaust pipe and flexpipe

After the treatment of the exhaust gas inside the catalytic converter, the concentration of soot and dangerous compounds is low enough to fulfill the restrictions of the environmental law EURO 5 99/96/EC.

This clean stream passes through the flexpipe and the exhaust pipe, which leads to a forced convection heat transfer between the exhaust gas and the inner wall of the pipe.

The flexpipe presents a ringed surfaced surrounded by a mesh made of stainless steel that is modeled in RadTherm by a three layers straight pipe as shown in Figure 22.

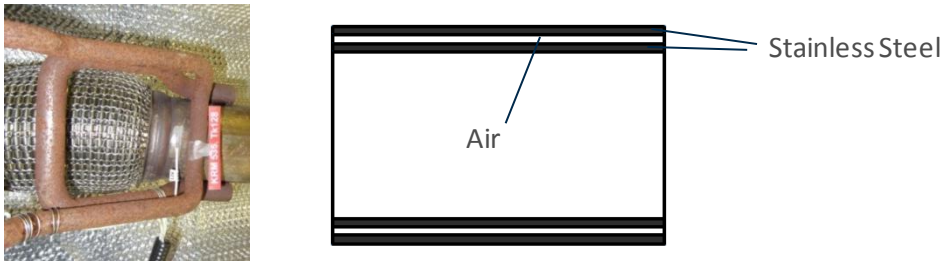

Figure 22. Comparison between the real flexpipe and the flexpipe modeled in RadTherm.

The gas inside the exhaust pipe is modeled in RadTherm as a stream by defining the inlet, the outlet and the direction of the flow. An advection link is required to connect this stream with the upstream fluid node.

As it was explained in the section 5.1, RadTherm calculates the heat transfer coefficient based on the correlations shown in Appendix A and multiply the value obtained by the CAF.

6.Results and discussion

Through this section the most relevant results are presented and discussed. The instrumentation and testing in the wind tunnel test are described in Section 6.1. Finally, in section 6.2 the results obtained from the model are compared against the tunnel test measurements.

6.1. Testing and Instrumentation

A driving case (HCTR70) was tested in the wind tunnel in order to validate the model described in this thesis. The HCTR70 is defined as a hill climb test with a 1600 kg trailer. The test is performed under a constant velocity of 70km/h and finishes when stable conditions are reached. The duration of the hill climb tests is usually set according to a specific distance; this means that the test is finished when the car has traveled a specific number of kilometers. However, the tunnel test used in this model was carried out until stable conditions were reached, ensuring that constant temperatures were achieved. The characteristic parameters of the tunnel test and the vehicle are shown Table 10.

Table 10.Hill climb tunnel test

Ambient Temperature (^{o}C)	27
Vehicle Speed (km/h)	70
Engine Speed (rpm)	2864
Engine Load (Nm)	244

The measuring data was sampled with Ipetroik logger, using uncalibrated K-type thermocouples. The inaccuracy of the K-type thermocouples depends on the temperature range; from -40^{o}C to 375^{o}C the inaccuracy is estimated to ± 2.1 °C, whereas for temperatures between 375^{o}C and 1000^{o}C it is estimated to be ± 6.5 °C.

The thermocouples were placed according to experience and some of them were covered with aluminum foil to counteract radiation effects.

6.2. Validation

This section shows and discusses the results obtained by coupling RadTherm and Fluent until convergence is reached. The model developed is able to predict surface temperature all around the engine. However, this section only focuses on the analysis of the exhaust surface temperature based on the elements labeled in Figure 23. Results for the complete engine are presented in Appendix D.

The temperature values from the tunnel test are compared with the simulation results based on the temperature of the mesh elements located in approximately the same positions as the thermocouples. The comparison of both temperature profiles is shown in Figure 24

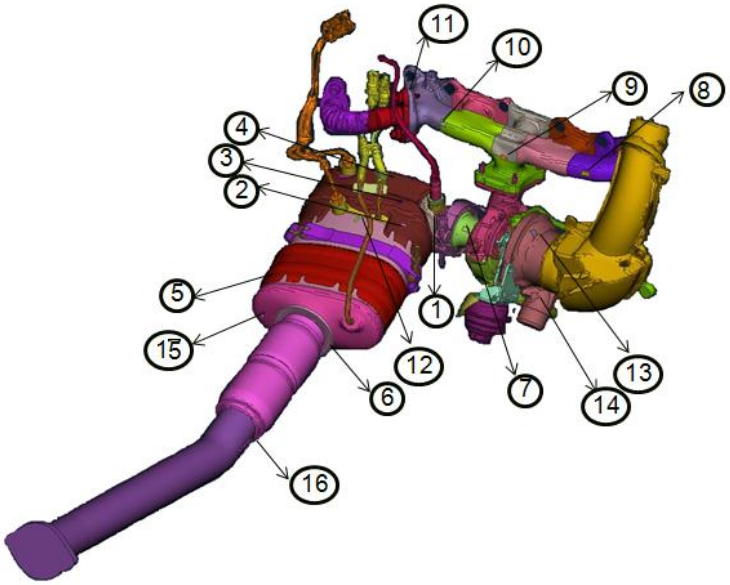

Figure 23. Instrumentation of the exhaust system

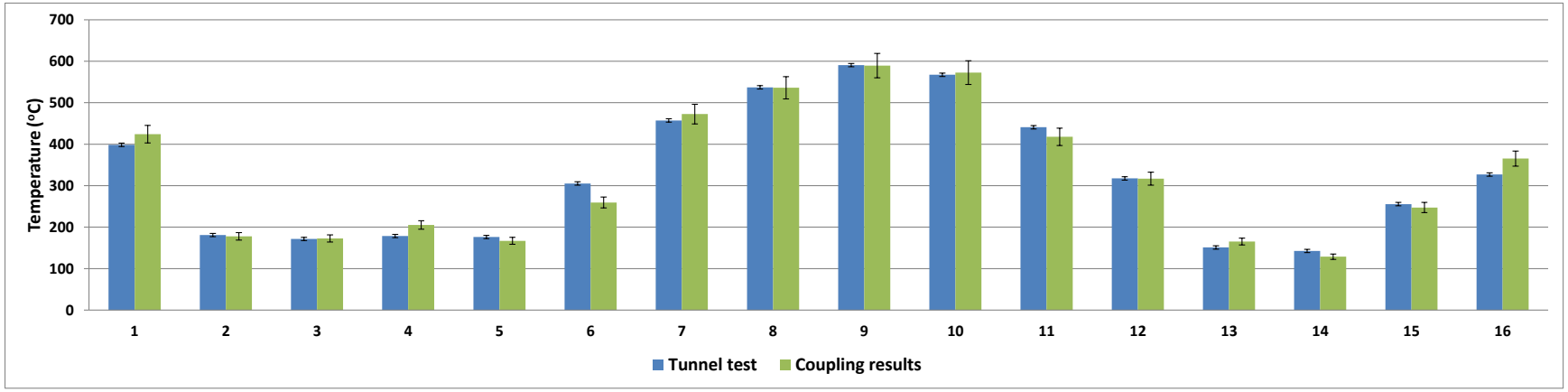

Figure 24. Comparison between the model results and the tunnel test data

A ±5% of error is illustrated in Figure 24 showing that only some points present a deviation higher than 5%. As seen in Figure 24 the developed model properly predicts the temperature tendency of the exhaust system even though there are some points that are not successfully predicted.

According to Figure 24, the highest deviation corresponds to element number 6 located in the catalytic cone out. Two thermocouples were placed in this part of the catalytic, as shown in Figure 23. The tunnel test shows that the gradient temperature between the thermocouple 6 and 15 is 50°C, whereas the model provides a gradient temperature of approximately 18°C. This deviation is likely be due to the reduction of the cross-sectional area where the gas flows from the catalytic cone out to the flexible pipe, which presents an area around five times lower than the catalytic converter. As explained in section 4, the gas inside the catalytic cone out is simulated as a fluid node which cannot simulate the flow acceleration because of the sharp change of the cross-sectional area.

Figure 24 also shows a high deviation between the model and the tunnel test data in thermocouple 16, located right after the flexible pipe. A possible reason for this deviation is that the geometry of the flexible pipe is not properly defined in RadTherm. The flexible pipe presents a ringed surface surrounded by a mesh made of stainless steel, although this geometry is not modeled in RadTherm. As described in section 5.4, this part of the flexpipe is modeled in RadTherm as a three layer straight pipe.

It is important to note that the temperatures shown in Figure 24 correspond to temperatures of mesh elements located close to the thermocouples, inducing some error, especially in areas with large temperature gradients. Both point 16 and point 6 are located on surfaces that present high temperature gradients, as seen in Figure 25.

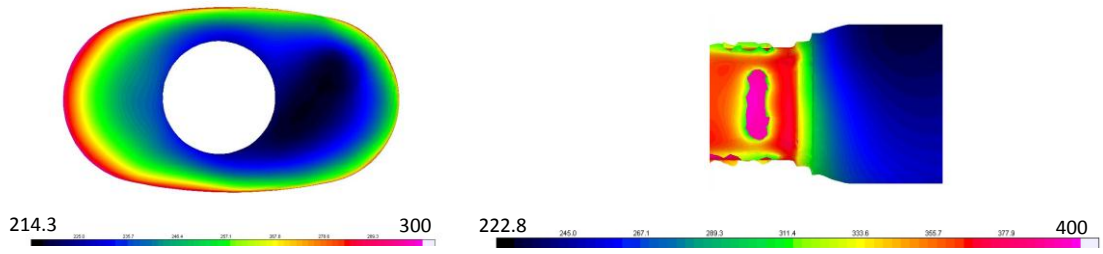

Figure 25. Temperature gradient in the cone out and downpipe surfaces

In the case of the point 7, by moving the element cell 5mm an increase around 20°C is reached, which shows the high influence of the element position on the results. Other points such as point 1, 4 and 11 are also located in areas with high temperature gradients which increase the deviation temperature

The model developed is able to predict the tendency of the temperature profiles of both the complete engine and the exhaust system as shown in Appendix D. However, some points present a temperature deviation higher than 20° C.

This deviation can be due to inaccuracy of the thermocouples and their positions. As explained before, the elements used in the thermal model may not be placed in the exact same positions as the thermocouples. For this reason, the temperature of elements located in areas with large gradients may not be the same as the temperature measured in the tunnel test.

It is important to note that in the model the flow inside the turbocharger is modeled as a fluid node instead of simulating the flow with CFD software. This means that the values used as the

internal heat transfer coefficient and the imposed work on the fluid node have a great influence on the predicted temperature in the turbocharger. Therefore, this can be considered as another source of error. This can also be applied for the catalytic converter where the flow is simulated as a fluid node.

Another parameter than can induce an error is the reaction heat imposed on the lumped capacitance, which depends on the exhaust gas concentration at the inlet of the DOC and the software used in the car. This concentration is really difficult to determine, so several measurements should be carried out to obtain a better estimation of this value. However, the HC and CO concentration used in the developed model was measured only once by the Aftertreatment Department, which may decrease the accuracy of the results.

It is also worth mentioning that the physical properties of the materials used in this model can introduce uncertainty into the results, especially the materials used as isolation. The physical properties used to define the materials in Radtherm are temperature dependent which might lead to some errors.

The local convection coefficients and the local fluid temperatures obtained by CFD simulations are influence by many parameters. The number of cells, the turbulence and wall functions are only some of the factors that may influence on the boundary conditions provide by Fluent.

7.Sensitivity analysis

A sensitivity analysis is required to evaluate the robustness of the model. The influence of several parameters on the simulation results is studied and described in this section. The simulations of the sensitivity analysis are carried out only in RadTherm to speed up the process.

7.1. Turbocharger work

As explained in section 5.2, the work in the turbocharger is imposed on the fluid nodes located inside the turbine and the compressor. The imposed work is given by the Powertrain department that calculates the work experimentally introducing certain error in the model.

In order to evaluate the influence of this parameter on the surface temperatures, simulations with different imposed work are performed. The imposed work used in case 1 is 15% higher than the reference value, whereas in case 2, the imposed work is reduced by about 15%.

Figure 26. shows a comparison between the reference and case 1 and 2.

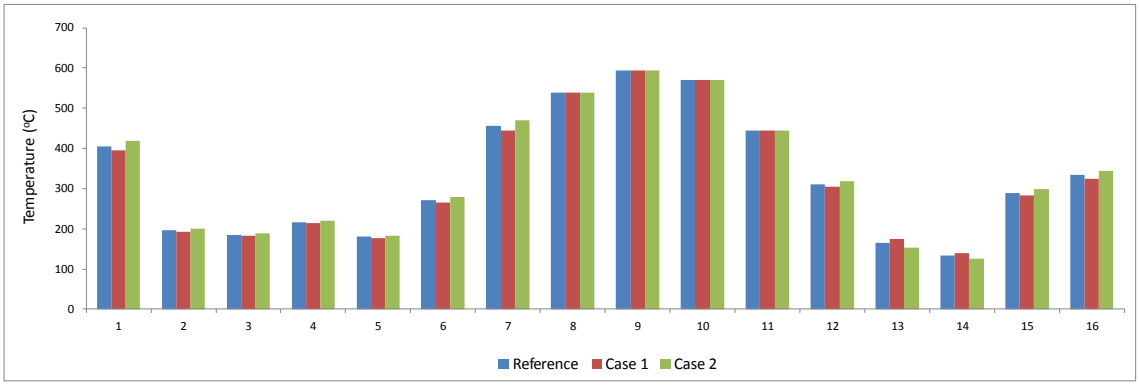

Figure 26. Comparison between reference results and Case 1 can Case 2.

By increasing the imposed work, lower temperatures are obtained over the whole exhaust system except for point 13 located on the compressor surface. The largest temperature deviations correspond to points 1, 7, 13 and 16 as shown in Figure 26. As expected, the temperatures of the components upstream of the turbocharger do not change.

The temperatures of points 1, 7 and 16 is about 10oC lower than the reference values due to the increase of the amount of energy removed from the fluid during the expansion inside the turbine. On the contrary, in case 1 the temperature of point 6 located in the compressor increases as a consequence of the augment of energy imposed on the air during the compression.

7.2. Reaction heat released inside the DOC

As explained in Section 5.3, the heat released during the reactions is imposed on the lumped capacitances located inside the DOC. The reaction heat depends on the concentration of HC and CO molecules in the gas at the inlet of the catalytic converter. This concentration is measured by the Aftertreament department. It is very difficult to properly estimate this concentration, so it is reasonable to include the gas concentration as a parameter in the analysis. A new case, Case 3, is simulated with higher HC concentration and lower CO concentration in the gas in comparison with the reference case. Results from both simulations are illustrated in Figure 27.

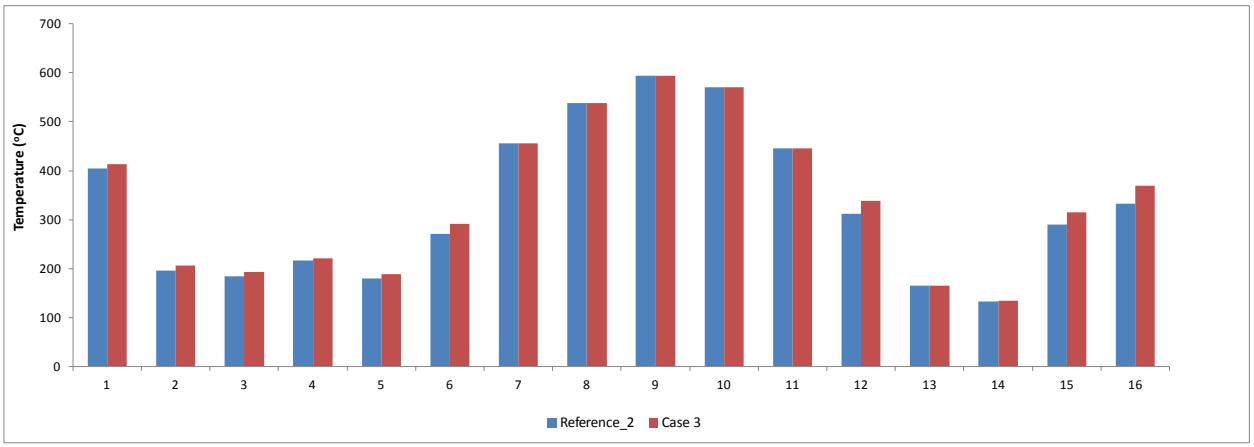

Figure 27. Comparison between reference results and Case 3.

As shown in Figure 27, in case 3 the temperatures of all the components after the turbocharger increase because of the augmentation of the energy released during the reactions. A rise of 800 ppm in the concentration of HC leads to an increase of around 20^{o}C in most of the points which demonstrates that the model is highly sensitive to the HC concentration.

7.3. Pressure drop inside the DOC and DPF

The pressure drop between the inlet and outlet of the DOC and DPF is measured and given by the supplier. The pressure drop depends on several parameters such as the number of particles retained in the surface, the gas mass flow rate and the smoothness of the surface. The energy of the gas inside the catalytic converter depends on the energy imposed on the fluid nodes, which is calculated based on the pressure drop.

Three cases are simulated with the following pressure drops.

- Case 4. Pressure drop applied in the DOC is equal to half the pressure drop used in the reference simulation.
- Case 5. Pressure drop applied in the DPF is equal to double the pressure drop used in the reference simulation.

- Case 6. Pressure drop applied in the DPF is equal to half the pressure drop used in the reference simulation.

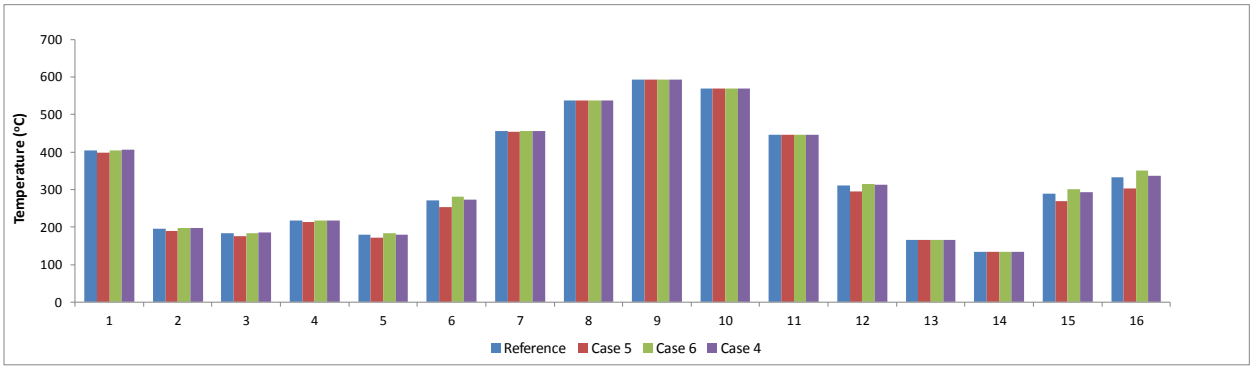

Figure 28. Comparison between reference results and Case 5, Case 6 and Case 7.

As illustrated in Figure 28, the pressure drop in the DOC presents a very low influence on the results. However, a change in the value of the pressure drop in the DPF leads to high temperature deviations especially for points 6, 12, 15 and 16.

The temperature variation due to the pressure drop is linear, showing a temperature change of around 1.2^{o}C per kPa.

7.4. Isolation properties

As mentioned in section 5.3, isolation mats are located around the catalytic converter in order to decrease the exhaust surface temperature. The isolation materials contained in this model are silica fiber and alumina fiber. These materials are defined in RadTherm by density, conductivity and specific heat. The conductivity is the parameter that presents the highest dependency with temperature, so it is reasonable to include the conductivity in the sensitivity analysis [13].

The reference case uses a conductivity equal to 0.2 W/mK whereas the conductivity applied in case 7 and case 8 is equal to 0.5 W/mK and 0.01 W/mK, respectively. Figure 29 shows a comparison between these cases and the reference case.

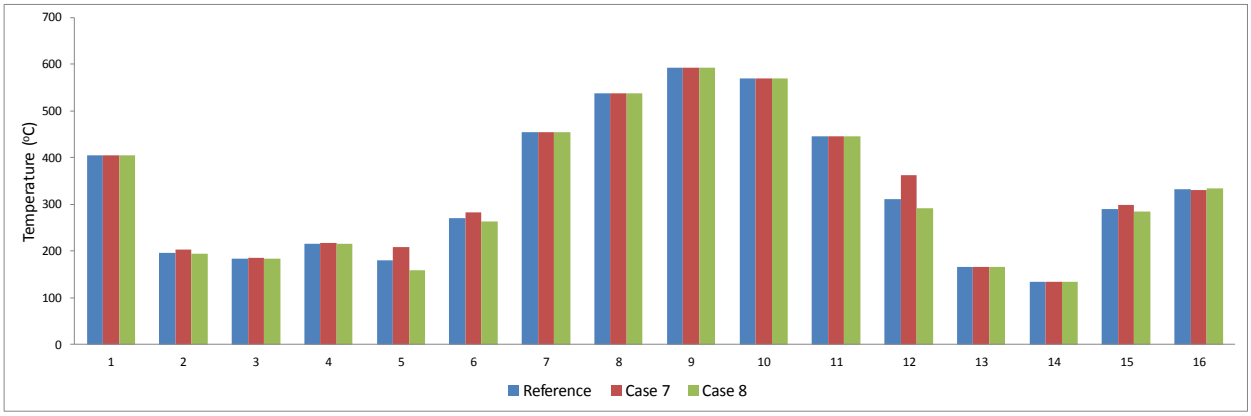

Figure 29. Comparison between reference results and Case 7 and Case8.

The heat transferred by conduction is directly proportional to the conductivity which means that an increase in the conductivity leads to high heat transfer rates. Figure 29 shows that an increase in the conductivity leads to higher temperatures, whereas lower temperatures are obtained when the conductivity is decreased, as expected.

The highest temperature differences correspond to points 5, 6, 11 and 15 which are located in the areas that contain isolation inside.

It can be observed that the relationship between the temperature and the conductivity is not linear. An increase in the conductivity leads to a higher temperature deviation from the reference in comparison to a decrease in the conductivity.

7.5. Contact resistance

As explained in Section 5.3, the contact resistance depends on the surface finish, the material, the pressure, the substance in the interstitial spaces, and the temperature [13]. This parameter is included in the sensitivity analysis due to the complexity of estimating a proper value.

Several cases varying the contact resistance are simulated and the results show that the contact resistance influence on the surface temperatures can be neglected. Appendix E contains a summary of all the cases simulated with difference contact resistance values.

7.6. Heat transfer coefficients

The convection heat rate is calculated based on the heat transfer coefficient applied in each part of the exhaust gas. Several assumptions regarding geometry and gas properties are required in order to estimate the heat transfer coefficient by correlations.

The influences of the heat transfer coefficients inside the turbine and the catalytic converter are evaluated within the sensitivity analysis. The values used in each case are summarized in Table 11.

Table 11. Heat transfer coefficients applied in each case

Heat transfer (W/m^2K)		**Reference**	**Case 13**	**Case 14**	**Case 15**	**Case 16**	**Case 17**	**Case 18**
Inside the turbine	Inlet	265	**850**	Ref.	Ref.	Ref.	Ref.	Ref.
	Volute	294	**1300**	Ref.	Ref.	Ref.	Ref.	Ref.
	Outlet	350	**700**	Ref.	Ref.	Ref.	Ref.	Ref.
	Clamp	188	**500**	Ref.	Ref.	Ref.	Ref.	Ref.
Inside the catalytic converter	Inlet	230	Ref.	**300**	Ref.	Ref.	Ref.	Ref.
	Inside DOC	220	Ref.	Ref.	**400**	Ref.	Ref.	Ref.
	Middle	201	Ref.	Ref.	Ref.	**250**	Ref.	Ref.
	Inside DPF	129	Ref.	Ref.	Ref.	Ref.	**400**	Ref.
	Cone_out	136	Ref	Ref	Ref	Ref	Ref	**250**

The results described in Appendix F show that the influence of the heat transfer coefficient can be neglected except in case 13 and case 14. In case 13 the temperatures of points 1 and 7 increase by about 10^{o}C and 17^{o}C, respectively. These points are located at the turbine outlet and the catalytic converter inlet so that they are highly affected by the internal convection heat transferred. An increase in the internal heat transfer coefficient leads to a larger convection heat transferred and higher temperatures are obtained.

In case 14, the increase of the heat transfer coefficient causes a 15^{o}C rise in the temperature of point 1. As explained before, this point is placed in the catalytic converter inlet which means that by applying a higher heat transfer coefficient, the heat transfer rate by convection increases and so does the surface temperature.

8.Conclusions

A thermal model was developed to be coupled with CFD software in order to obtain the surface temperature in the exhaust system and the nearby engine components.

Even though several assumptions were made during the development of the method, the model demonstrated that coupling CFD software with heat transfer software can successfully predict the surface temperatures.

Throughout the whole method described in this thesis, the components have been analyzed separately, according to correlations that better fit with each component, to increase the accuracy of the model. This approach provided a greater understanding on the effect of individual influences and more flexibility in the variation of parameters and correlations of the model.

The pulsating nature of the exhaust gas introduces large levels of turbulence that increase the heat transfer rates inside the system. This phenomenon was simulated in the model by using a convective augmentation factor (CAF) equal to 2.5.

The high thermal activity of the catalytic converter was well simulated through imposing heat on the lumped capacitance and fluid nodes. The developed model has control over the catalytic pressure drop and reaction heat based on the concentration of the exhaust gas.

A sensitivity analysis was performed in order to evaluate the robustness of the method. The influence of some factors in the steady-state solution is evaluated during the analysis. From this study, it is concluded that the most critical parameter in the model are:

- The imposed work
- The reaction heat
- The pressure drop
- The isolation properties

That means that this modeling process can be applied to other driving cases as long as the critical values are properly adjusted according to the new case being studied.

This model was validated against a tunnel test, revealing that the model is able to predict the temperature tendencies of the exhaust system and the nearby surrounding engine components. The temperature profiles obtained from the steady-state simulations match closely with the tunnel test data, considering the possible sources of error and discrepancies.

In conclusion, this thesis showed the feasibility of coupling a thermal model with a CFD model to successfully simulate the temperature of some engine components. This modeling process allows modifying the design without involving new experimental tests, contributing to a reduction in both time and cost. Consequently, this method will be used in future projects within the VCC verification efficiency processes.

9.Future work

The first future task is to increase the complexity of the thermal model by including the muffler and EGR system within the model. Furthermore, the same methodology applied in the DOC may be used to simulate the heat released during the regeneration of the DPF.

The simulation results are validated against the tunnel test data for one driving case (HCTR70). Therefore, the next step is to simulate a top speed case.

The method development described in this thesis properly predicts the temperature tendency of the exhaust system under steady-state conditions. Therefore, the next task is to extend from steady-state to transient conditions in order to simulate more realistic driving cases

The modeling process may be improved in the future as follows,

- Determination of the optimal number of loops during the coupling.
- Modeling the internal flow of the gas in the turbocharger and catalytic converter by CFD software.
- Sensitivity analysis of the parameters used in CFD simulations.

10. References

[1] J.Tu, G.H. Yeah, C. Liu "Computational Fluid Dynamics. A practical Approach," 2008.

[2] F. P. Incropera. a. D. P. Dewit, "Fundaments of Heat and Mass Transfer," 2011.

[3] G. Nellis. a. S. Klein, "Fundaments of Heat and Mass Transfer," 2009.

[4] A. Stamatelos. I.P. Kandylas, "Engine exhaust system design based on heat transfer computation," 1998.

[5] T. Heuber. H. Többen. P. Zacke. D. Chatterjee. O. Deutschmann. a. J. Warnatz. Joachim Braun, "Influnence of Physical and Chemical Parameters on the Conversion Rate of a Catalytic Converter: A Numerical Simulation Study,", no. 2000-01-0211, 2000.

[6] F. Lacin. a. M. Zhuang, "Modeling and Simulation of Transient Thermal and Conversion Characteristics for Catalytic Converters," no. 2000-01-0209, 2000.

[7] R. Martínez-Botas. Alessandro Romagnoli, "Heat transfer analysis in a turbocharger turbine: An experimental and computational evaluation," vol. 38, 2012.

[8] J. F. P. Chesse, A. Miboom, M. Cormearais, "Heat Transfer Analysis in a Turbocharger Compressor: Modeling and Experiments," Detroit, Michigan, 2006.

[9] K. D. Wygant,. A. Driss. Nick Baines, "The Analysis of Heat Transfer in Automotive Turbochargers," vol. 132, no. 042301-1, 2010.

[10] Depcik, C., and Assanis, D., "A universal Heat Transfer Correlation for Intake and Exhuast Flows ina a Sparl-Ignition Internal Combustion Egine," no. 2002-01-0372, 2002.

[11] Bauer, W.-D., Wenisch J., and Heywood, J. B. "Averaged and Timer-Resolved Heat Transfer of Steady and Pulsating Entry Flow in Intake Manifold of a Spark-Ignition Engine".

[12] V. R. Lakkireddy, J. H. Johnson. a. S. T. Bagley. Hasan Mohammed, "An experimental and Modeling Study of a Diesel Oxidation Catalyst and a Catalyst Diesel Particulate Filter Using a 1-D 2-Layer Model," no. 2006-01-0466, 2006.

[13] J. H. Liengard, A heat transfer textbook, Massachussetts: Phlogisto Press, 2002.

Appendix A

RadTherm correlations to calculate heat transfer coefficients.

Duct, Laminar Flow (Re<100)

$$h = (\frac{k}{D_h})(\frac{3.66 + 0.85Grz}{1 + 0.047Grz^{2/3}})(\frac{\mu_b}{\mu_w})^{0.14} \qquad \text{(A1)}$$

where μ_b is the fluid viscosity at the bulk (fluid) temperature and the μ_w is the fluid viscosity at the wall temperature. Grz is the Graez number.

$$Gz = \frac{1}{L^*} = \frac{D_h \cdot \mathrm{Re}_{D_h} \mathrm{Pr}}{L}. \qquad \text{(A2)}$$

Duct laminar Flow (100<Re<2100)

$$h = 1.86\left(\frac{k}{D_h}\right)(Grz)^{1/3}(\frac{\mu_b}{\mu_w})^{0.14} \qquad \text{(A3)}$$

Duct, Transient flow (2100<Re<10000)

$$h = 0.118\left(\frac{k}{D_h}\right)(\mathrm{Re}^{2/3} - 125)(\mathrm{Pr})^{1/3}(1 + (\frac{D_h}{L})^{2/3})(\frac{\mu_b}{\mu_w})^{0.14} \qquad \text{(A4)}$$

Correlations provided by Gnielinksi (1976)

$$Nu_{D_h, fd} = \frac{(\frac{f_{fd}}{8})(\mathrm{Re}_{D_h} - 1000)\mathrm{Pr}}{1 + 12.7(\mathrm{Pr}^{2/3} - 1)\sqrt{\frac{f_{fd}}{8}}} \quad \text{for } 0.5 < \mathrm{Pr} < 2000 \text{ and } 2300 < \mathrm{Re}_{Dh} < 5 \cdot 10^6 \text{ (A5)}$$

where f_{fd} is the fully developed friction factor and is provided by Petukhov (1970),

$$f_{fd,h,e} = \frac{1}{[0.790\ln(\mathrm{Re}_{D_h}) - 1.64]^2} \quad \text{for } 3000 < \mathrm{Re}_{Dh} < 5.0 \cdot 10^6 \qquad \text{(A6)}$$

The average Nusselt number cn be approximately computed according to (Kakaç et al. (1987)) when the flow is not fully developed:

$$Nu_{D_h} \approx Nu_{D_h, fd}[1 + C(\frac{x}{D_h})^{-m}] \qquad \text{(A7)}$$

Where reasonable values of the constant C and m are 1.0 and 0.7 (3).

Correlations provided by Hornbeck (1965)

$$Nu = 3.66 + \frac{\left[0.049 + \frac{0.02}{\mathrm{Pr}}\right] Gz^{1.12}}{\left[1 + 0.065 Gz^{0.7}\right]} \qquad \text{(A8)}$$

Correlations provided by Shah and Lond (1978)

$$Nu_{D_h}, T_{fd} = 7.541(1 - 2.610AR + 4.97AR^2 - 5.119AR^3 + 2.702AR^4 - 0.548AR^5) \quad \text{(A9)}$$

where AR is Aspect Ratio which is the ratio of the minimum to the maximum dimensions.

Appendix B

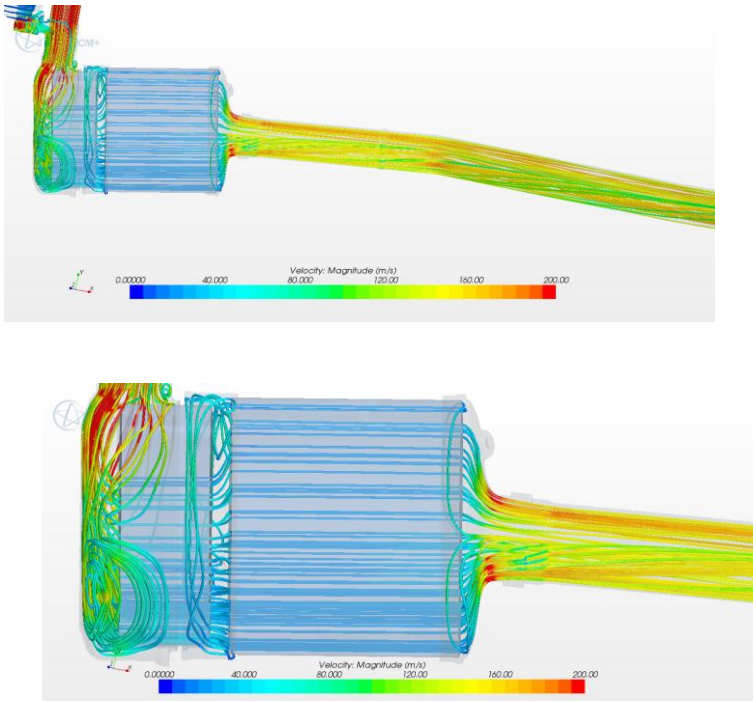

Figure 30. Velocity distribution

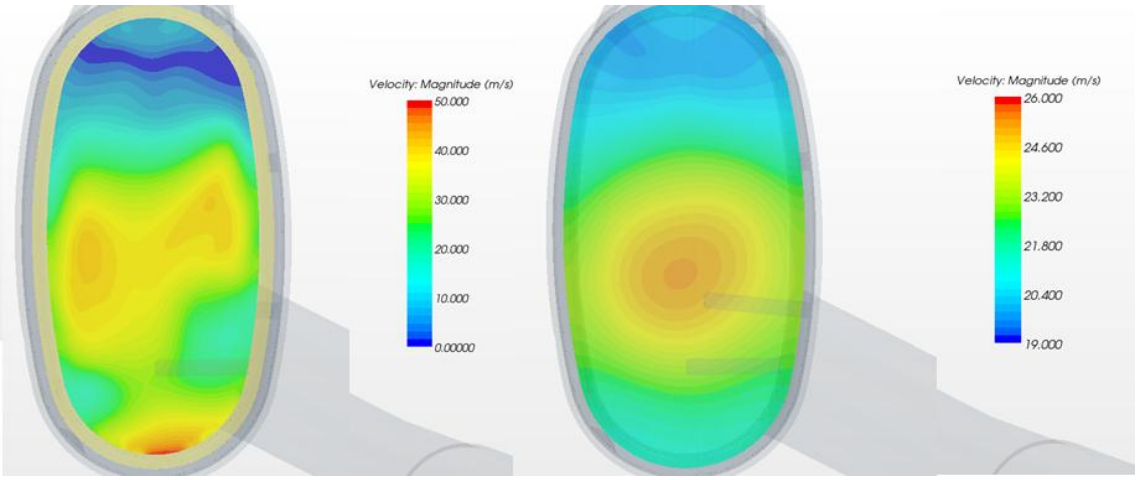

Figure 31. Axial velocity and Uniformity index in the middle of the susbtrate

Appendix C

Substrate inside the diesel oxidation catalyst

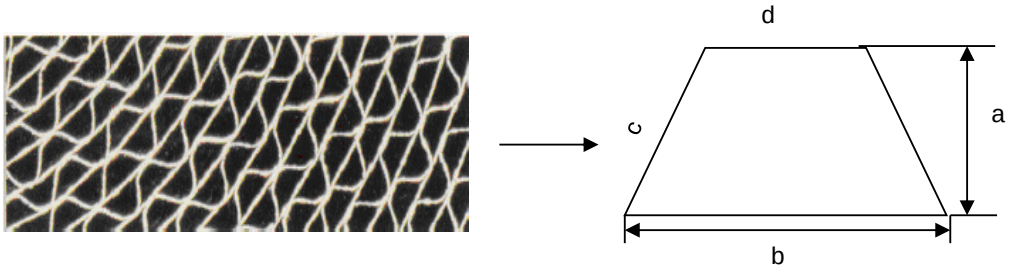

$$A_{cells} = A_{frontal} / n_{cells} \quad \text{(B1)}$$

$$n_{cells} = A_{frontal} \cdot cpsi \quad \text{(B2)}$$

$$A_{cells} = a_{ext} \cdot b_{ext} \quad \text{(B3)}$$

Assuming that b≈2a,

$$A_{cells} = 2 \cdot a_{ext}^{\ 2} \quad \text{(B4)}$$

The internal dimensions are calculated as follows,

$$a_{\text{int}} = a_{ext} - t \quad \text{(B5)}$$

$$b_{\text{int}} = 2a_{\text{int}} \xrightarrow{d_{in} \approx a_{\text{int}}} c_{\text{int}} = a_{\text{int}}\sqrt{2} \quad \text{(B6)}$$

$$A_{\text{int}} = a_{in_t} \cdot b_{\text{int}} \quad \text{(B7)}$$

$$P_{cell} = b_{\text{int}} + d_{\text{int}} + 2c_{\text{int}} \quad \text{(B8)}$$

$$A_{gas\_flow} = P_{cell} \cdot Length \quad \text{(B9)}$$

$$A_{lumped} = A_{gas\_flow} \cdot n_{cells} \quad \text{(B10)}$$

$$m_{lumped} = m_{matrix} + m_{\text{covering}} \quad \text{(B11)}$$

$$A_{lumped_i} = \frac{A_{lumped}}{3} \quad \text{(B12)}$$

$$m_{lumped_i} = \frac{m_{lumped}}{3} \quad \text{(B13)}$$

$$A_{lumped_i} = 21759{,}22mm^2 \quad \text{(B14)}$$

$$m_{lumped_i} = 835.43cm^3 \quad \text{(B15)}$$

Filter inside the diesel particulate filter

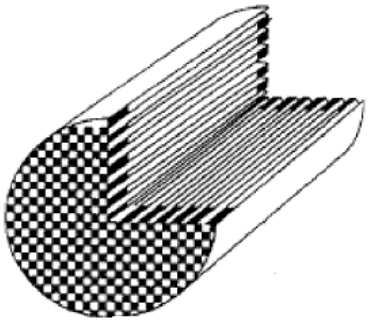

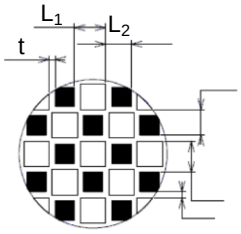

$$n_{cells} = A_{frontal} \cdot cpsi \quad \text{(B16)}$$

$$A_{cells} = a_{ext} \cdot b_{ext} \quad \text{(B17)}$$

$$L_{filter} = L_{filter} - plug \quad \text{(B18)}$$

$$L_{\text{int}} = \frac{(L_1 + L_2)}{2} \quad \text{(B19)}$$

$$A_{\text{int}} = L_{\text{int}}{}^2 \qquad P_{\text{int}} = 4 \cdot L_{\text{int}} \quad \text{(B20)}$$

$$V_{cells} = A_{\text{int}} \cdot L_{filter} \cdot n_{cells} \quad \text{(B21)}$$

$$A_{lumped} = L_{filter} \cdot P_{\text{int}} \cdot n_{cells} \quad \text{(B22)}$$

$$V_{lumped} = V_{total} - V_{holes} \quad \text{(B23)}$$

$$A_{DPF} = 25707.96mm^2 \quad \text{(B24)}$$

$$V_{DPF} = 2663.24cm^3 \quad \text{(B25)}$$

Reaction heat and pressure drop

$$Q_{reaction} = moles_{C_3H_6} \cdot \Delta H_{reaction} + moles_{C_3H_6} \cdot \Delta H_{reaction} \quad \text{(B26)}$$

where moles are the mol flow rate (mol/s) and ΔH is given is J/s.

Assuming a100% of efficiency in both reactions,

$$moles_{gas} = \frac{\dot{m}_{gas}}{3} \cdot 10^{-6} \cdot moles_{gas} \quad \text{(B27)}$$

$$moles_{C_3H_6} = \frac{[ppmHC]}{3} \cdot 10^{-6} \cdot moles_{gas} \quad \text{(B28)}$$

$$moles_{CO} = \frac{(\%vol/vol)}{100} \cdot moles_{gas} \quad \text{(B29)}$$

$$Q_{lumped\_i} = x_i \cdot Q_{reaction} \quad \text{(B30)}$$

$$Heat\_losses = \dot{V}_{exhaust\_gas} \cdot \Delta P_{substrate} \quad \text{(B31)}$$

Where the $\dot{V}_{exhaust\_gas}$ is given in m^3/s and the ΔP in Pa.

$$Heat\_losse_{node\_i} = x_i \cdot Total\_heat\_losses \quad \text{(B32)}$$

Appendix D

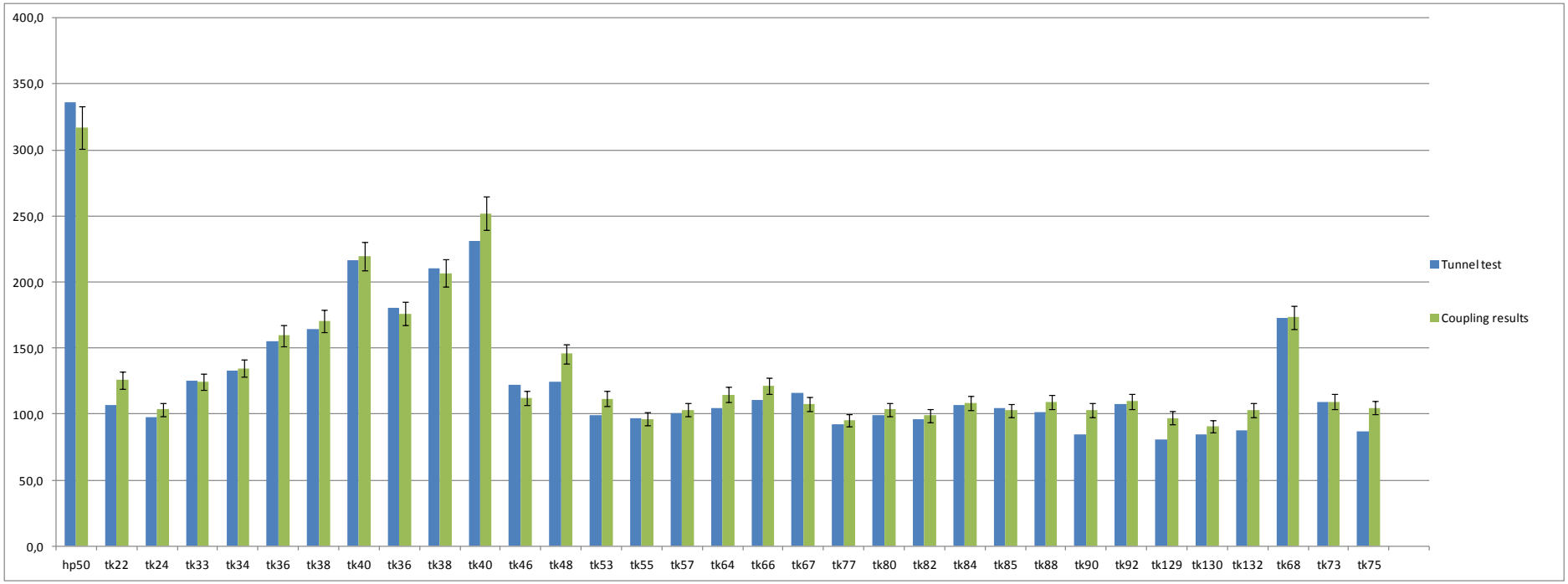

Figure 32. Temperatures of the nearby surrounding engine components obtained by coupling

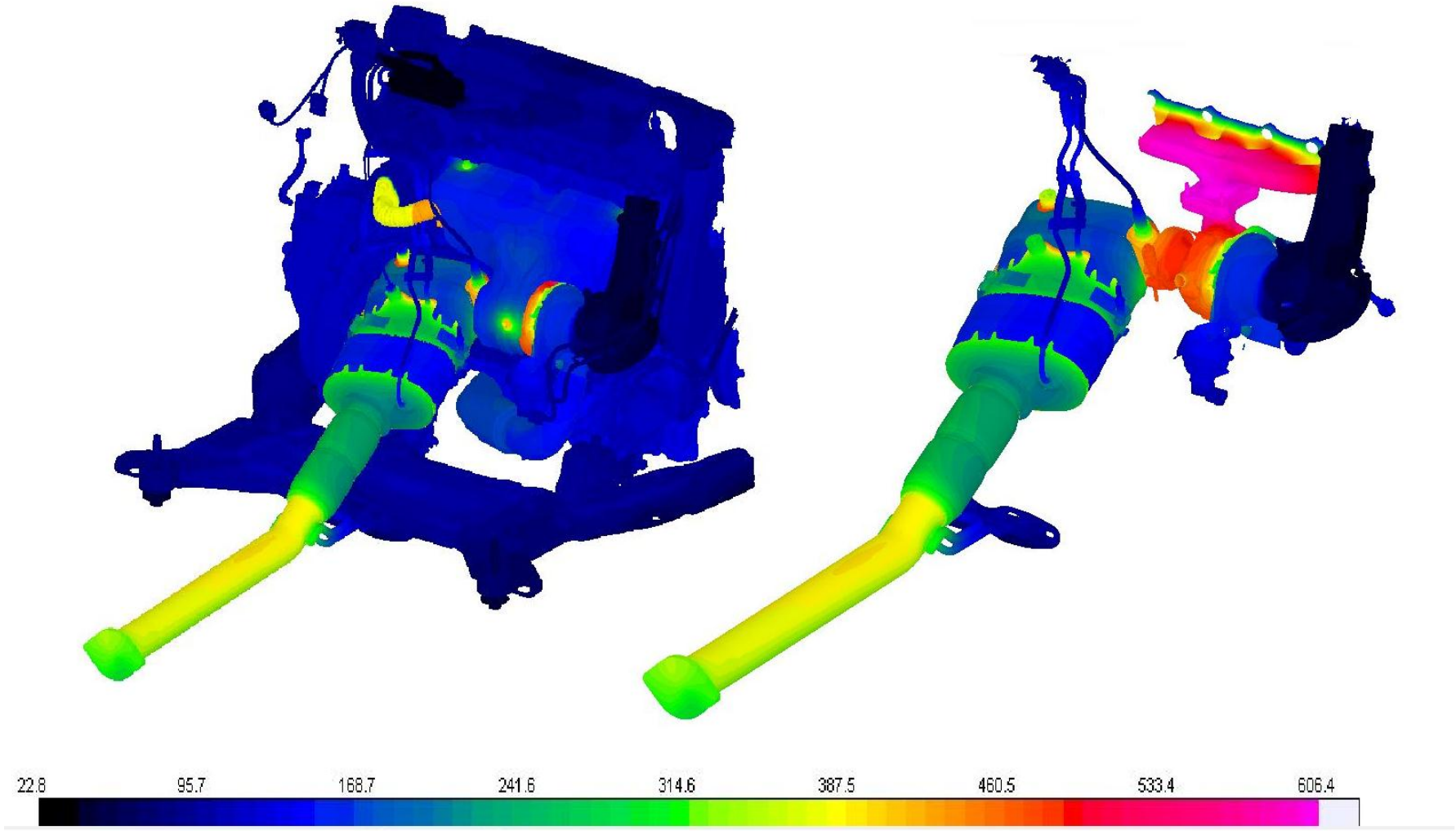

Figure 33. Temperature profile of Temperatures of the exhaust system and nearby surrounding engine components

Appendix E

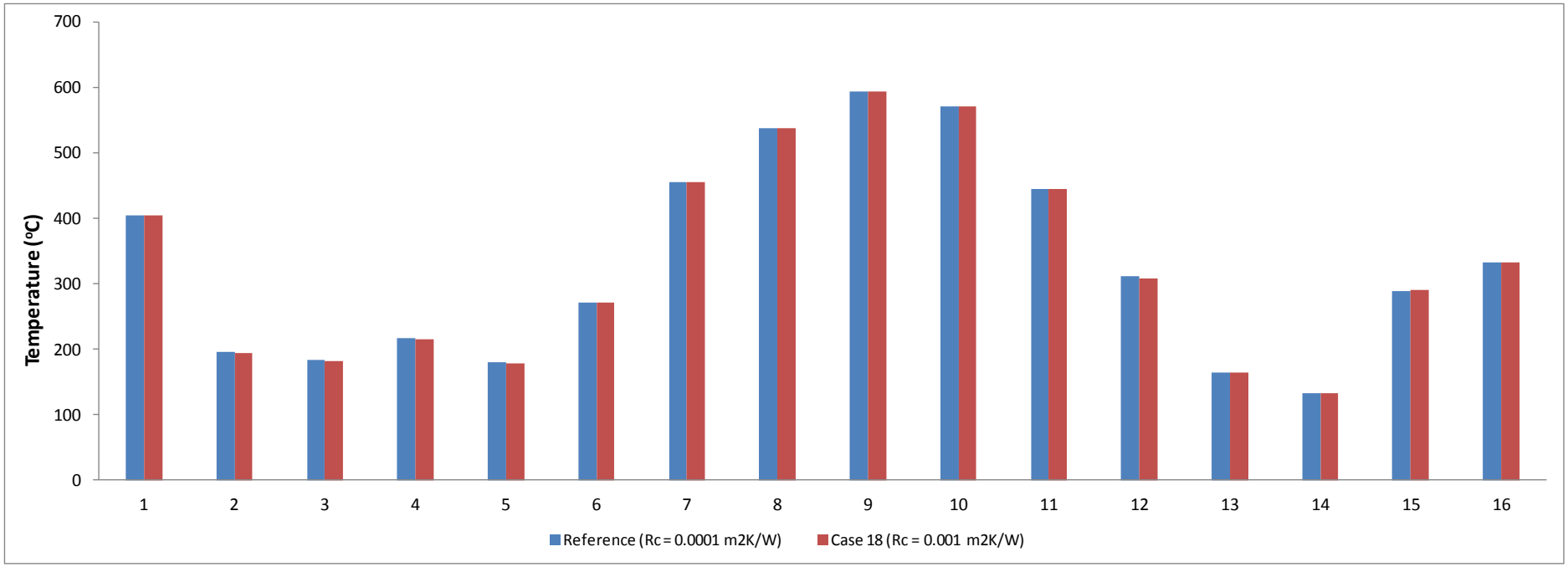

Figure 34. Comparison between results obtained applying different values of contact resistance of the catalytic heat shield

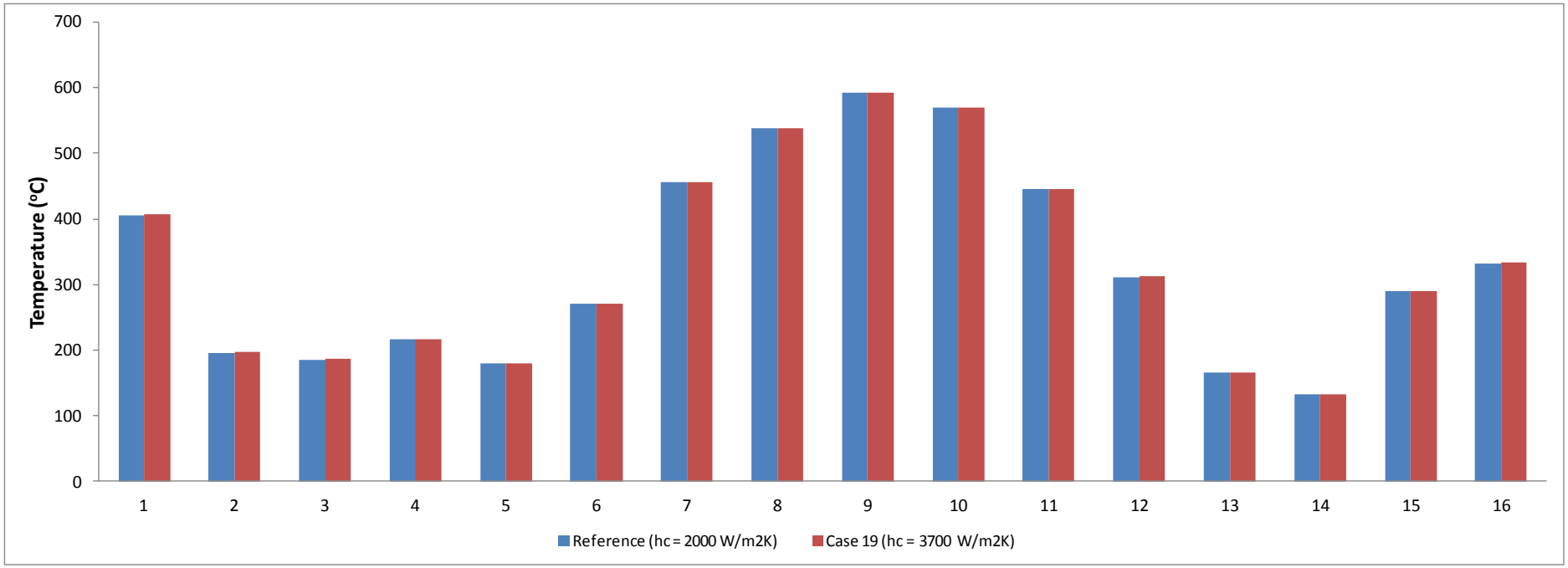

Figure 35. Comparison between results obtained applying different values of contact resistance of the DOC substrate

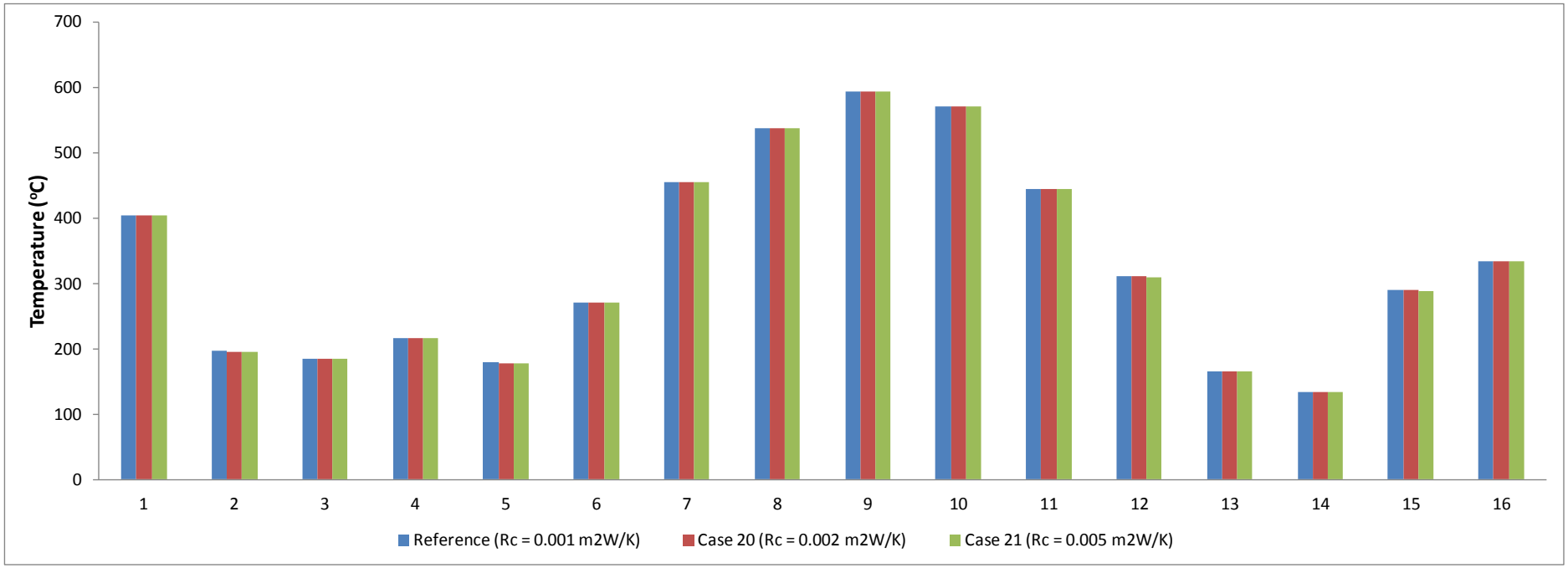

Figure 36.Comparison between results obtained applying different values of contact resistance of the DPF

Appendix F

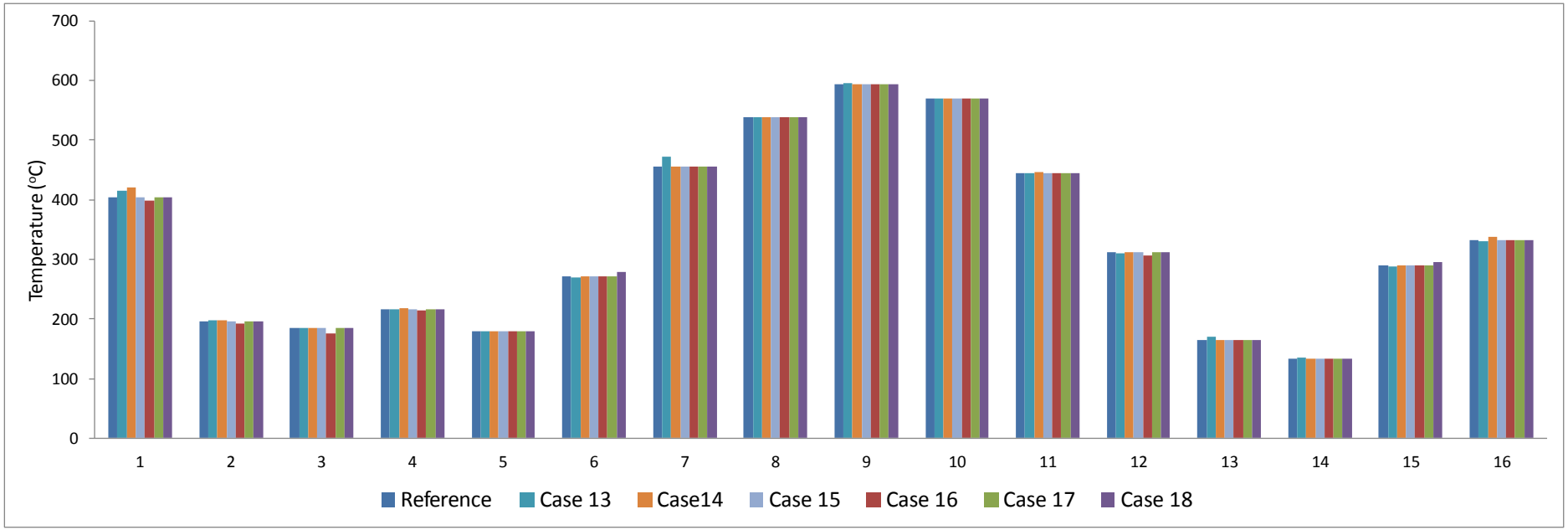

Figure 37. Comparison between reference results and Case 13-18